Resource

Cell Reports

Circadian and Feeding Rhythms Orchestrate the Diurnal Liver Acetylome

Graphical Abstract

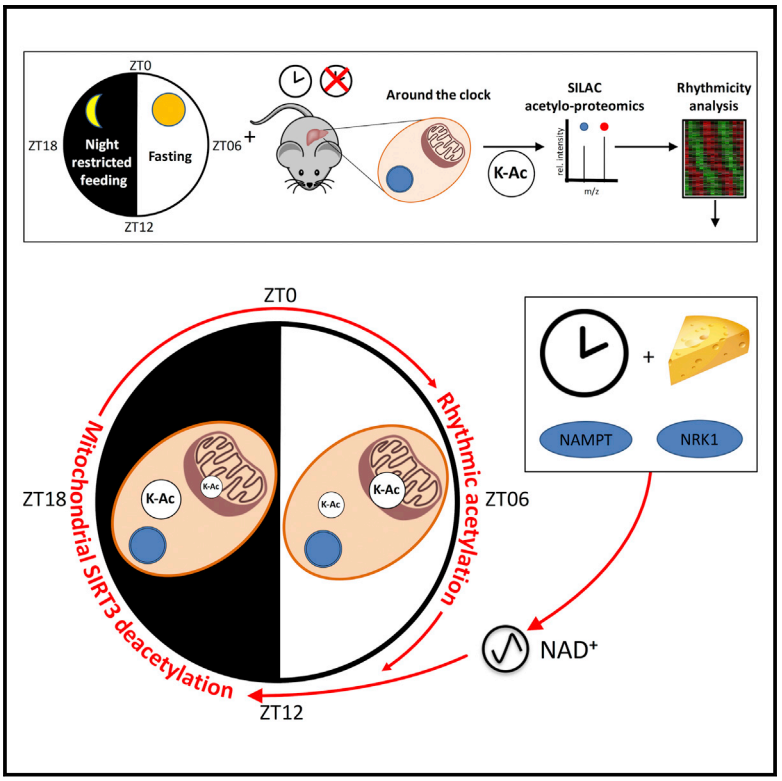

Authors

Daniel Mauvoisin, Florian Atger, Loïc Dayon, ..., Martin Kussmann, Felix Naef, Frédéric Gachon

Correspondence

frederic.gachon@rd.nestle.com

In Brief

Mauvoisin et al. provide a rhythmic acetylome map of the mouse liver. Rhythmic acetylated proteins showed subcellular localization-specific phases with an over-representation of SIRT3 targets. Feeding rhythms and the circadian clock regulate NAD^+ synthesis through the salvage and nicotinamide riboside pathways, affecting metabolite accumulation.

Highlights

- Phase of daily acetylated proteins is subcellular localization-dependent
- Mitochondrial proteins are over-represented among the rhythmically acetylated proteins
- Acetylated mitochondrial protein are enriched in SIRT3 targets
- Circadian clock regulates the NAD^+-dependent SIRT3 activity through the NR pathway

Accession Numbers

PXD005317
PXD005310

Mauvoisin et al., 2017, Cell Reports *20*, 1729–1743
August 15, 2017
http://dx.doi.org/10.1016/j.celrep.2017.07.065

Cell Reports
Resource

Circadian and Feeding Rhythms Orchestrate the Diurnal Liver Acetylome

Daniel Mauvoisin,[1,2] Florian Atger,[1,3,8] Loïc Dayon,[4,8] Antonio Núñez Galindo,[4,8] Jingkui Wang,[2,6,8] Eva Martin,[1] Laetitia Da Silva,[4] Ivan Montoliu,[4] Sebastiano Collino,[4] Francois-Pierre Martin,[4] Joanna Ratajczak,[1,5] Carles Cantó,[1,5] Martin Kussmann,[4,7] Felix Naef,[2] and Frédéric Gachon[1,5,9,*]

[1]Diabetes and Circadian Rhythms Department, Nestlé Institute of Health Sciences, 1015 Lausanne, Switzerland
[2]Institute of Bioengineering, School of Life Sciences, Ecole Polytechnique Fédérale de Lausanne, 1015 Lausanne, Switzerland
[3]Department of Pharmacology and Toxicology, University of Lausanne, 1015 Lausanne, Switzerland
[4]Systems Nutrition, Metabonomics & Proteomics, Nestlé Institute of Health Sciences, 1015 Lausanne, Switzerland
[5]School of Life Sciences, Ecole Polytechnique Fédérale Lausanne, 1015 Lausanne, Switzerland
[6]Present address: Research Institute of Molecular Pathology, Campus Vienna Biocenter 1, 1030 Vienna, Austria
[7]Present address: The Liggins Institute, University of Auckland, New Zealand
[8]These authors contributed equally
[9]Lead Contact
*Correspondence: frederic.gachon@rd.nestle.com
http://dx.doi.org/10.1016/j.celrep.2017.07.065

SUMMARY

Lysine acetylation is involved in various biological processes and is considered a key reversible post-translational modification in the regulation of gene expression, enzyme activity, and subcellular localization. This post-translational modification is therefore highly relevant in the context of circadian biology, but its characterization on the proteome-wide scale and its circadian clock dependence are still poorly described. Here, we provide a comprehensive and rhythmic acetylome map of the mouse liver. Rhythmic acetylated proteins showed subcellular localization-specific phases that correlated with the related metabolites in the regulated pathways. Mitochondrial proteins were over-represented among the rhythmically acetylated proteins and were highly correlated with SIRT3-dependent deacetylation. SIRT3 activity being nicotinamide adenine dinucleotide (NAD)$^+$ level-dependent, we show that NAD$^+$ is orchestrated by both feeding rhythms and the circadian clock through the NAD$^+$ salvage pathway but also via the nicotinamide riboside pathway. Hence, the diurnal acetylome relies on a functional circadian clock and affects important diurnal metabolic pathways in the mouse liver.

INTRODUCTION

Lysine acetylation on proteins has been shown to broadly regulate diverse sets of cellular functions (Choudhary et al., 2009). Understanding the dynamics of protein acetylation in regulating cellular pathways is therefore key to deciphering its biological functions (Smith and Workman, 2009). However, comprehensive analysis of lysine acetylation is technologically achievable only recently, using antibodies recognizing acetylated lysine residues (Kim et al., 2006). To date, only a few studies have described further acetylome maps in mammals. Early studies identified hundreds of acetylated peptides in the liver, with a strong enrichment in mitochondrial proteins (Kim et al., 2006; Schwer et al., 2009; Zhao et al., 2010). More recently, multi-organ studies identified thousands of acetylated peptides in rodents, opening new avenues regarding the regulation of acetylation and its effect on cellular functions, including metabolism (Lundby et al., 2012; Yang et al., 2011). Descriptions of mechanisms involved in regulating such acetylation, mainly through enzymatically controlled deacetylation, are rising and strongly linked to metabolism and physiological conditions (Menzies et al., 2016). However, the dynamics of protein acetylation are still poorly described, despite the currently known regulation by food-related metabolites and nutrient availability.

Through the regulation of diurnal feeding rhythms and nutrient metabolism, the circadian clock is likely an important modulator of protein acetylation. The circadian clock, an endogenous and autonomous oscillator with a nearly 24-hr period, coordinates most aspects of physiology and behavior in mammals (Gerhart-Hines and Lazar, 2015). This oscillatory clockwork is organized in a hierarchical manner, with a master clock in the suprachiasmatic nuclei of the hypothalamus that communicates timing cues to downstream oscillators in peripheral tissues. At the molecular level, rhythms in gene expression are generated by interconnected transcriptional and translational feedback loops in which multiple layers of control, including temporal, transcriptional, post-transcriptional, and post-translational regulation, play important roles (Crane and Young, 2014). Although efforts have been conducted in the last decade to comprehensively study transcriptional regulation orchestrated by the circadian clock, regulation at the proteome level is still largely unexplored territory, despite recent advances in the field (Mauvoisin et al., 2014; Neufeld-Cohen et al., 2016; Robles et al., 2014; Wang et al., 2017). Evidence also indicates that the circadian clock is a key regulator of deacetylase activity, affecting mitochondrial

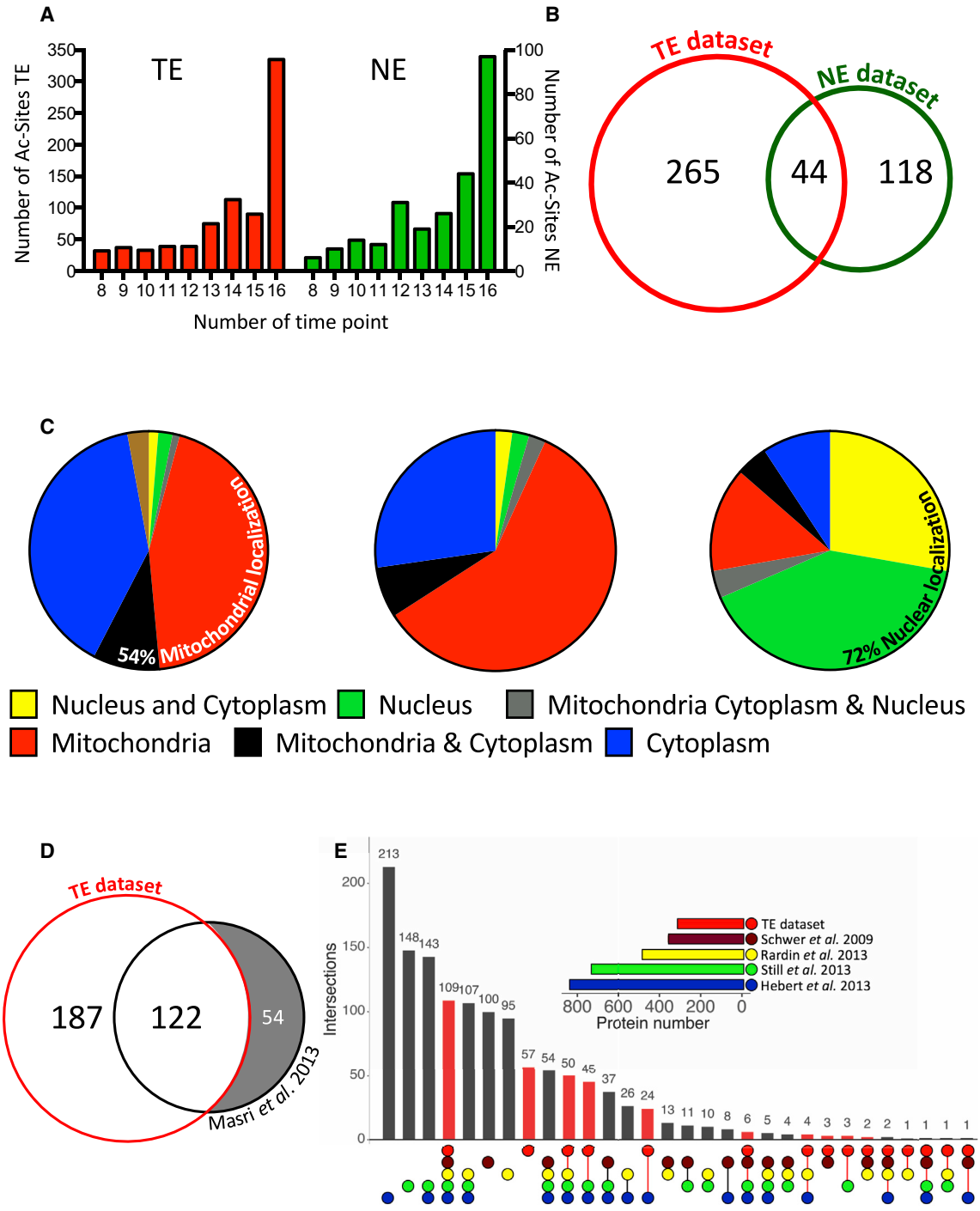

Figure 1. Characterization of the Liver Acetylome

(A) Distribution of sample number for the quantified acetylation sites in TE (red bars plotted on the left y axis) and NE (green bars plotted on the right y axis).

(B) Venn diagram showing the number of acetylated proteins quantified in TE (red circle, 309 acetylated proteins identified) and NE (green circle, 162 acetylated proteins identified).

(C) Distribution of cellular localization of proteins with quantified acetylation sites in TE (left), TE and NE (center), and NE (right). Data are expressed in percent.

(D) Venn diagram comparing the TE dataset of acetylated proteins with the previous circadian liver acetylome (Masri et al., 2013) (176 unique acetylated proteins identified).

(legend continued on next page)

function (Peek et al., 2013). However, little is known about the global diurnal acetylome, despite the recent description of 19 diurnally acetylated sites in wild-type (WT) mouse liver (Masri et al., 2013). Using optimized sample preparation, including antibody-based enrichment protocols combined with sensitive nano-reverse-phase liquid chromatography (RP-LC) tandem MS (MS/MS) applied to total (TE) and nuclear (NE) mouse liver protein extracts harvested during two diurnal cycles, we were able to detect 1,831 and quantified 1,050 acetylated sites, of which around 13% presented a diurnal acetylation pattern. These acetylated proteins are characterized by a bimodal distribution of peak times. Proteins acetylated during the night are enriched in cytoplasmic and nuclear proteins, whereas proteins acetylated during the day are enriched in mitochondrial proteins. This rhythm in mitochondria is associated with the activity of the nicotinamide adenine dinucleotide $(NAD)^+$-dependent SIRT3 deacetylase. Rhythmic acetylated proteins are involved in several key metabolic pathways, and metabolite levels within these pathways correlated with acetylation levels. Of interest is that the diurnal distribution of acetylation and metabolites is highly disturbed in clock-disrupted animals such as *Bmal1* knockout (KO) and *Cry1/2* double knockout (DKO) mice, mainly through the differential regulation of NAD^+ synthesis, supporting a crucial role of the circadian and feeding rhythms in finely tuning the diurnal liver acetylome.

RESULTS

The Acetylome of the Mouse Liver

To obtain further insights into the diurnal acetylation in mouse liver, we performed an in vivo stable isotope labeling by amino acids (SILAC) MS-based proteomic experiment in which TE and NE protein extracts were collected every 3 hr during two consecutive days under light-dark conditions and night-restricted feeding. After trypsin digestion, these extracts were enriched for acetylated peptides (Experimental Procedures). Relative acetylated peptide abundance in the resulting 16 TE and 16 NE samples was quantified using a common SILAC total or nuclear reference extract, respectively (Figure S1A), whose labeling efficiency has already been reported (Mauvoisin et al., 2014). This experimental setup allowed the identification of 1,298 lysine acetylation sites in TE and 533 in NE, of which 236 unique sites were commonly detected in both datasets (Figure S1B; Table S1). The reproducibility of our experiment was high because the correlation between biological replicates was 76% on average (Figure S1C). Moreover, as a proxy of nuclear enrichment quality, 75% of the obtained raw MS signal in NE originated from acetylated peptides of nuclear proteins (Figure S1D). For further analysis, only acetylation sites yielding relative quantitative measurements in at least 8 of the 16 samples were considered. Additionally, only sites with a previously quantified accumulation of the corresponding protein in TE (Mauvoisin et al., 2014) and NE (Wang et al., 2017) were retained (Figure 1A; Table S2). Using such criteria, 797 acetylation sites within 309 proteins in TE and 253 acetylation sites within 162 proteins in NE were quantified (Figure 1B; Table S2). In TE, the majority of identified and quantified acetylation sites originated from cytoplasmic and mitochondrial proteins, whereas the NE dataset was enriched in acetylation sites from nuclear proteins and proteins shuttling between the cytoplasmic and nuclear compartments (Figure 1C; Figure S1D). In total, 44 proteins were found acetylated in both datasets, likely proteins shuttling between different organelles or dually targeted proteins that can be present in different compartments, as reported for mitochondrial/nuclear proteins (Figure 1C; Monaghan and Whitmarsh, 2015). Comparison of our datasets (Table S2) with the previously published diurnal acetylome performed on whole liver extracts under ad libitum feeding (Masri et al., 2013) showed that, besides our increased coverage, which is more than doubled, our quantified TE acetylome includes 70% of the aforementioned data (Figure 1D). Additional comparisons of this dataset with published mitochondrial liver acetylomes (Hebert et al., 2013; Rardin et al., 2013a; Schwer et al., 2009; Still et al., 2013) showed that 70% of our acetylated proteins were present in at least two of these datasets, corroborating the enrichments for mitochondrial proteins in our liver acetylome (Figure 1E). The remaining non-overlapping proteins are likely cytoplasmic or nuclear proteins that are not present in theses mitochondrial datasets.

The Rhythmic Acetylome of the Mouse Liver

We next identified actively acetylated lysine by analyzing the rhythmicity of the acetylation signal normalized by its corresponding protein signal (Mauvoisin et al., 2015; Experimental Procedures; Table S2). Using this relative acetylation signal, we first observed that most of the rhythmic acetylated peptides are found on non-rhythmic proteins, which characterize an active acetylation process. Hence, we found 133 rhythmic acetylated lysines ($p < 0.05$), 106 in TE and 27 in NE and 3 of them found in both datasets (Figure S2A; Table S2). These rhythmic sites were found in 73 unique proteins in TE (including 8 rhythmic at the protein level; Mauvoisin et al., 2014), 23 in TE (including 13 rhythmic at the protein level in the nucleus; Wang et al., 2017), and 2 proteins common between TE and NE. The proportion of about 13% of rhythmic acetylated sites is higher compared with the previously published liver diurnal acetylome (19 rhythmic acetylation sites in the WT, about 6% of the dataset; Masri et al., 2013), probably because of the higher coverage and time resolution as well as the feeding schedule in the present study. Comparing the intersection between the two datasets revealed a minor overlap; only 5 acetylation sites were found in common in both studies (Figure S2A). We additionally identified acetylation sites with a 12-hr period: 34 sites within 30 proteins in

(E) Matrix layout for all intersections (vertical bars), sorted by size, of our TE dataset, with the data from studies performed using liver mitochondrial protein extract: Schwer et al. (2009) (356 acetylated proteins), Rardin et al. (2013b) (483 acetylated proteins), Still et al. (2013) (729 acetylated proteins), and Hebert et al. (2013) (834 acetylated proteins). Color-coded circles in the matrix indicate sets that are part of the intersection and, the top horizontal bar graph displays the protein number for each study.

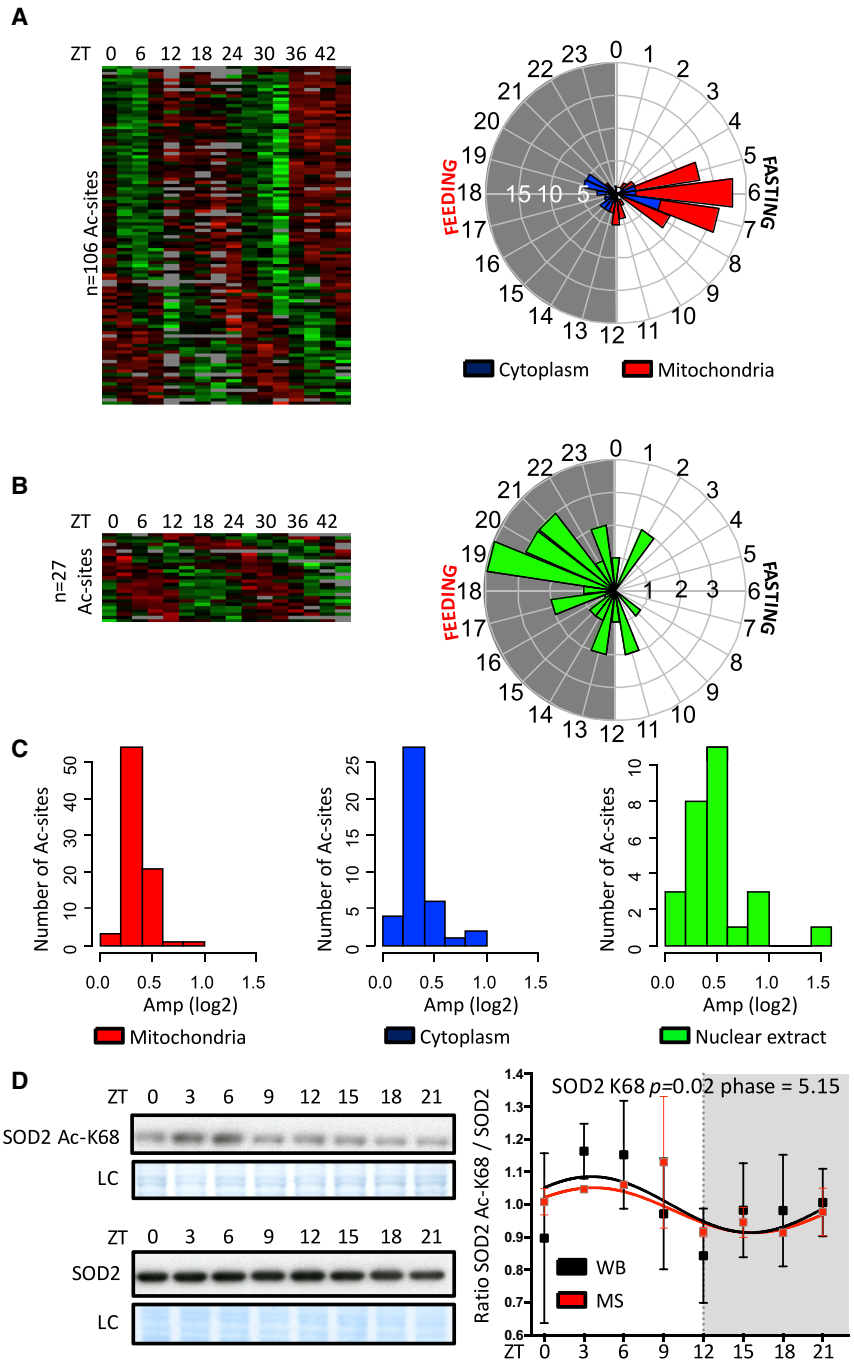

Figure 2. Rhythmicity Analysis of the Liver Acetylome

(A–C) Heatmaps showing rhythmic acetylation sites normalized by their corresponding total protein amount in TE (A) and NE (B) under light/dark and night-restricted feeding conditions. Data were standardized by rows, and gray blocks indicate missing protein data. The polar plots on the right of each heatmap display peak phase distribution of the rhythmic acetylation (Ac) sites, and (C) shows amplitude. The colors of the polar plots (A and B) and histograms (C) indicate Ac sites that have a corresponding total protein with a defined mitochondrial (n = 80 Ac sites, red) or cytoplasmic (n = 40 Ac sites, blue) localization or Ac sites that are identified in NE (n = 27 Ac sites, green).

(D) Western blot (WB) analysis of total protein extracts using acetyl-K68 SOD2 (top blot) or total SOD2 (bottom blot). MS data in red, mean ± SEM, are from Table S2. WB data in black, mean ± SEM, are from three independent biological samples and represent the ratio of the acetyl-K68 SOD2 signal on the total SOD2 signal. Data (MS and WB) are normalized to the temporal mean. Naphtol blue black staining of the membranes was used as a loading control (LC) and served as a reference for normalization of the quantified values.

TE and 17 sites within 14 proteins in NE (Figures S2B and S2C; Table S2).

Using protein localization databases, we annotated the cellular localization of all the rhythmic acetylated sites. Surprisingly, clear localization-specific phases were observed. Although mitochondrial proteins were acetylated during the day, when nutrient and energy are depleted, cytoplasmic and nuclear proteins were preferentially acetylated during the night, when nutrients are available at high levels (Figures 2A and 2B).

Compared with other post-translational modifications, such as rhythmic phosphorylation (Robles et al., 2017; Wang et al., 2017), despite a few high amplitudes of acetylation sites observed in the nucleus and mitochondria, we found that the amplitudes of rhythmic acetylation were relatively low. This could reflect the fact that acetylation/deacetylation are low-stoichiometry reactions (Weinert et al., 2015) compared with phosphorylation (Wu et al., 2011). Moreover, only a small fraction of the pool of proteins is subjected to acetylation on lysine, leading to the observed global low change on acetylation levels (Figure 2C). Validation of rhythmic acetylation of mitochondrial superoxide dismutase 2 (SOD2) at lysine 68 (Chen et al., 2011) was performed by western blot and presented similar diurnal variation as found by MS (Figure 2D).

Acetylation is acknowledged in general as a passive process mainly regulated by the availability of acetyl-coenzyme A (CoA) and counteracted by the regulated orchestration of deacetylation (Choudhary et al., 2014). In mammalian cells, acetyl-CoA concentration is not homogeneous. Indeed, its synthesis and accumulation are cell compartment-specific (Siess et al., 1978) and regulated by feeding/fasting cycles (Shi and Tu, 2015). For instance, during the fasting period, a 10-fold higher concentration of acetyl-CoA was observed in

the mitochondria, where it is synthetized from acetate by acetyl-CoA synthetase 2 (ACECS2, encoded mainly by the *Acss3* gene in the mouse liver) (Verdin et al., 2010). In contrast, lower concentrations were found in the cytoplasm and the nuclear compartments, where acetyl-CoA is produced from mitochondrially derived citrate by ATP citrate lyase (ACLY) or from acetate by acetyl-CoA synthetase 1 (ACECS1, encoded by the *Acss2* gene in the mouse) during feeding time (Wellen and Thompson, 2012). Remarkably, the observed compartment-specific rhythmic acetylation is well correlated with this food-driven acetyl-CoA synthesis in the respective compartment.

Although ACSS3 is not rhythmically expressed in TE or liver mitochondria (Neufeld-Cohen et al., 2016), ACSS2 and ACLY (Figures S2D and S2E), with the latter being highly expressed compared with other ACSS isoforms (Figures S2F and S2G), presented a synchronized diurnal accumulation in the mouse liver in both TE and NE. The maximum of expression of these acetyl-CoA-producing enzymes occurred during the light period in TE and at the night-day transition in NE, when cytoplasmic and nuclear acetylation levels were low (Figures 2A and 2B; Figures S2D and S2E). Proteomic data from circadian clock-disrupted mice in TE showed a minor disturbance of ACLY and ACSS2 expression (Figure S2H). Although ACSS3 expression was increased in *Bmal1* KO mice, it was previously shown that acetyl-CoA concentration is not affected in this model (Peek et al., 2013).

Together, these data are in line with the fact that lysine acetylation is mainly driven by passive acetylation caused by food-driven fluctuation of acetyl-CoA availability in their respective cell compartments; i.e., day in mitochondria and night in the cytoplasmic and nuclear compartments (Shi and Tu, 2015). The expression levels of acetyl-CoA-producing enzymes as well as the circadian clock components appear to weakly affect this diurnal compartment-specific regulation of acetyl-CoA level in a normal feeding regimen, as already shown (Chavan et al., 2016; Peek et al., 2013). However, the mitochondrial acetylation peak phase is likely followed by sirtuin-dependent deacetylation events in the opposite phase. Sirtuin-dependent deacetylation has been shown to be clock-regulated (Peek et al., 2013) and could be involved in the observed rhythmic acetylation.

The Rhythmic Acetylome Is Modulated by Circadian Clock-Orchestrated Rhythmic Deacetylation

Previously published results suggest that rhythmic deacetylation by sirtuins is likely involved in establishment of the rhythmic acetylome (Peek et al., 2013). Among sirtuins, SIRT2 is present mainly in the cytosol, whereas SIRT6 and SIRT7 are located in the nucleus. SIRT1 shuttles between the cytosol and the nucleus and is therefore involved in deacetylation within these two organelles (Menzies et al., 2016). Although SIRT4 (Mathias et al., 2014) and SIRT5 (Du et al., 2011) have very little deacetylase activity, SIRT3 is likely the main mitochondrial deacetylase. Of interest is that SIRT3-deacetylated proteins have been extensively studied in different mouse tissues and, notably, in the liver (Dittenhafer-Reed et al., 2015; Hebert et al., 2013; Lombard et al., 2007; Rardin et al., 2013b; Weinert et al., 2015). Many characterized targets of SIRT3 presented a rhythmic acetylation in our dataset, with a clear phase preference during the day, synchronized with rhythmically acetylated proteins in the mitochondria (Figures 3A and 3B; Table S3). In contrast, non-SIRT3 targets displayed a bimodal maximum of acetylation during the middle of the day and night, mostly synchronized with cytoplasmic and nuclear proteins. This observation was confirmed by the fact that most rhythmic SIRT3 targets are mitochondrial proteins, whereas the majority of rhythmic non-SIRT3 targets are localized in the cytoplasm, where they can be deacetylated by another unidentified deacetylase (Figure 3C). The 12-hr acetylation sites we identified were not enriched in SIRT3 targets compared with 24-hr acetylation rhythms (Figure S3A), suggesting that SIRT3 is not implicated in implementing 12-hr rhythms of acetylation. Remarkably, as described previously (Asher et al., 2008; Wang et al., 2017), SIRT1 and its activator RPS19BP1 (Kim et al., 2007), as well as SIRT2 and SIRT7, are rhythmic and synchronized in the nuclear compartment, with a maximum of accumulation during the night-day transition, after the peak of acetylation in this organelle (Figures S3B–S3D), and could therefore also be involved in this deacetylation process.

NAD^+ Synthesis and the Diurnal Acetylome Are Regulated by the Circadian Clock and the Feeding Schedule

As recently shown, the diurnal activity of SIRT3 is regulated by the circadian clock-regulated NAD^+ salvage pathway through the transcriptional control of nicotinamide phosphoribosyltransferase (*Nampt*), whose expression level peaks at the day-night transition (Nakahata et al., 2009; Peek et al., 2013; Ramsey et al., 2009). However, the level of NAD^+ appeared to be only partially related to *Nampt* expression, with the feeding regimen playing an important role in rhythmic NAD^+ accumulation. Under fasting conditions, liver rhythmic NAD^+ levels are maximal during the day (Peek et al., 2013), whereas they are biphasic under ad libitum feeding (Ramsey et al., 2009). The strong influence of feeding schedule on NAD^+ accumulation was additionally confirmed by mathematical modeling (Woller et al., 2016). Hence, in addition to clock disruption, the feeding schedule also appears to be a key player that fine-tunes NAD^+ diurnal oscillations. Hepatic NAD^+ production originates mainly from the amidated route (Mori et al., 2014), which includes the aforementioned NAD^+ salvage pathway involving NAMPT but also the nicotinamide riboside (NR) pathway. This NR pathway synthesizes NAD^+ from the dietary supplies of NR and nicotinamide mononucleotide (NMN) and involves nicotinamide riboside kinase 1 (NRK1), encoded by the *Nmrk1* gene (Ratajczak et al., 2016). In addition, the existence of organelle-specific NAD^+ biosynthesis enzymes also suggests that the regulation of NAD^+ pools is organelle-specific. Indeed, in the cytosol and the nucleus, NAD^+ is likely the product of NMN conversion by NMNAT1 and 2, whereas synthesis of the mitochondrial pool involves NMNAT3 (Cambronne et al., 2016). This suggests that the availability of NAD^+ precursors during the feeding period may affect the rhythmic deacetylation through rhythmic activation of sirtuins, and not only the circadian clock via the regulation of NAMPT expression.

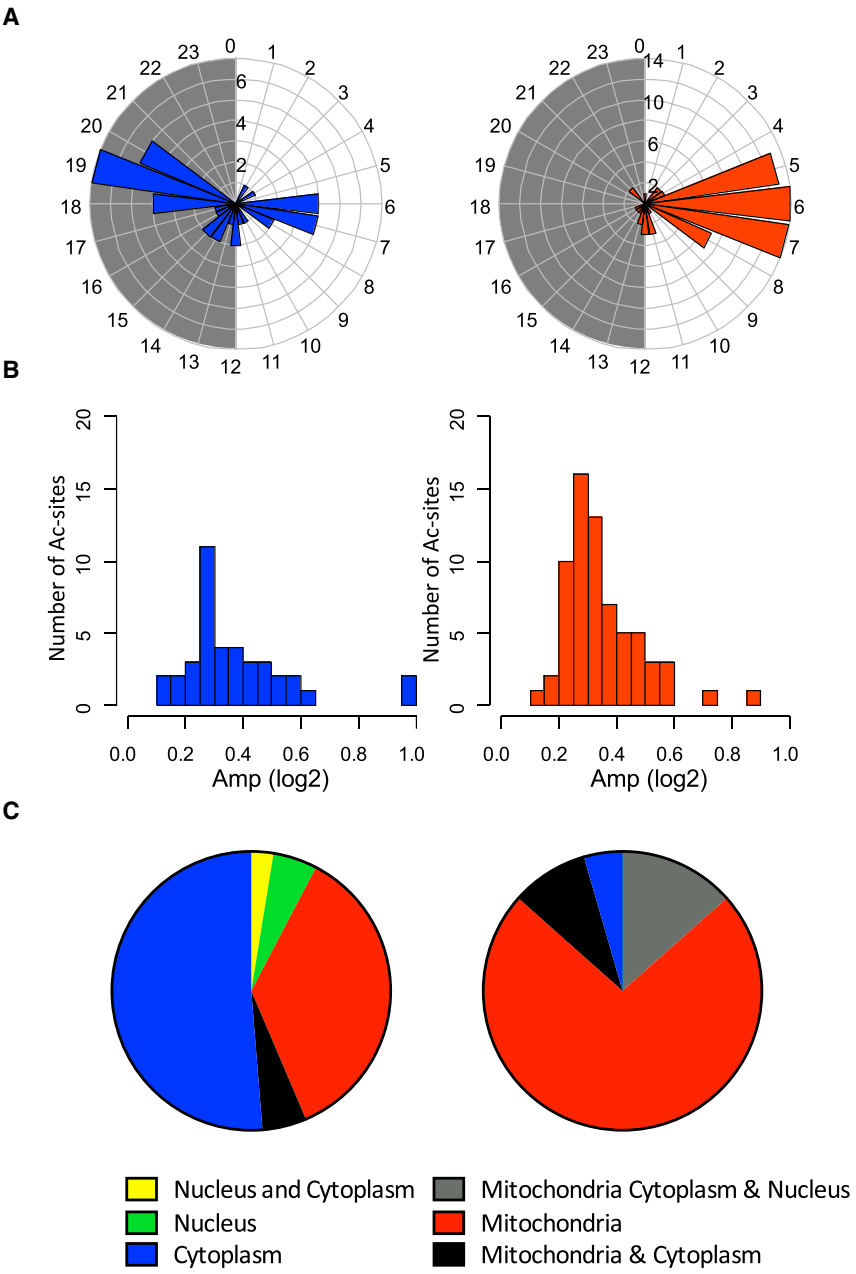

Figure 3. Rhythmic Behavior of Non-SIRT3 and SIRT3 Targets

(A–C) Peak phase (A), amplitude (B), and cellular localization (C) of rhythmic acetylation sites non-targeted (left) or targeted (right) by the SIRT3 deacetylase. Acetylation sites were defined as targeted by SIRT3 when their levels were significantly upregulated in *Sirt3* KO mice in Rardin et al. (2013b); Hebert et al. (2013), or Dittenhafer-Reed et al. (2015) (Table S3).

To test this hypothesis, we first investigated the effect of the circadian clock on rhythmic global acetylation by studying lysine acetylation in liver extracts from *Cry1/2* and *Bmal1* KO mice that present an inactivated circadian clock (Storch et al., 2007; van der Horst et al., 1999). As shown in Figure 4A, global acetylation was slightly decreased in *Cry1/2* DKO mice but increased in *Bmal1* KO mice. This change in global acetylation could therefore reflect the regulation of NAD^+ synthesis by the circadian clock and its associated regulation of sirtuin activity. Accordingly, we observed higher and lower NAD^+ levels in the livers of *Cry1/2* DKO and *Bmal1* KO mice, respectively, showing that the clock indeed controlled NAD^+ synthesis (Figure 4B). As mentioned before, although the circadian clock regulation of NAD^+ synthesis through the NAD^+ salvage pathway seems to be active under fasting conditions (Peek et al., 2013) or for cell-autonomous synthesis of NAD^+ (Nakahata et al., 2009), feeding-related pathways likely affect NAD^+ synthesis. We therefore speculated about the regulation of NAD^+ synthesis by the clock through the nutrient-dependent NR pathway. The genes encoding NAMPT and NRK1 as well as NMNAT3 presented a rhythmic expression at the mRNA level (Figure 4C). Although *Nampt* expression was, as described, perturbed in clock-disrupted mice (Figure 4C), this was also the case for *Nmrk1* at both the mRNA and protein levels (Figures 4C and 4D). However, *Nmnat3* expression as well as that of the non-rhythmic *Nmnat1* were not significantly affected in clock-disrupted mice (Figure 4C), whereas *Nmnat2* is not expressed in mouse liver.

To test whether the circadian clock directly regulates these genes, we took advantage of the recently published report regarding rhythmic genome-wide binding of circadian clock regulators (Koike et al., 2012) to study their binding on these specific genes. Interestingly, similar to the rhythmic binding of BMAL1 and NPAS2 around CT8 and the PER and CRY proteins at CT16 on the *Nampt* promoter, the promoter of *Nmrk1* was bound by BMAL1, CLOCK around CT6, and PER2 around CT16. Although BMAL1, CRY1, and CRY2 also bound the promoter of *Nmnat3* around CT0 and PER2 bound at CT16, they have apparently minor effect on its expression (Figure 4E), which is likely regulated by additional transcription factors regulated by food-derived signals, potentially contributing to its dysregulation observed in obesity (Drew et al., 2016; Jukarainen et al., 2016). Taken together, these results highlighted the fact that not only the NAD^+ salvage pathway but also the feeding-related NR pathway are influenced by the circadian clock and that both play an important role in clock-regulated NAD^+ synthesis.

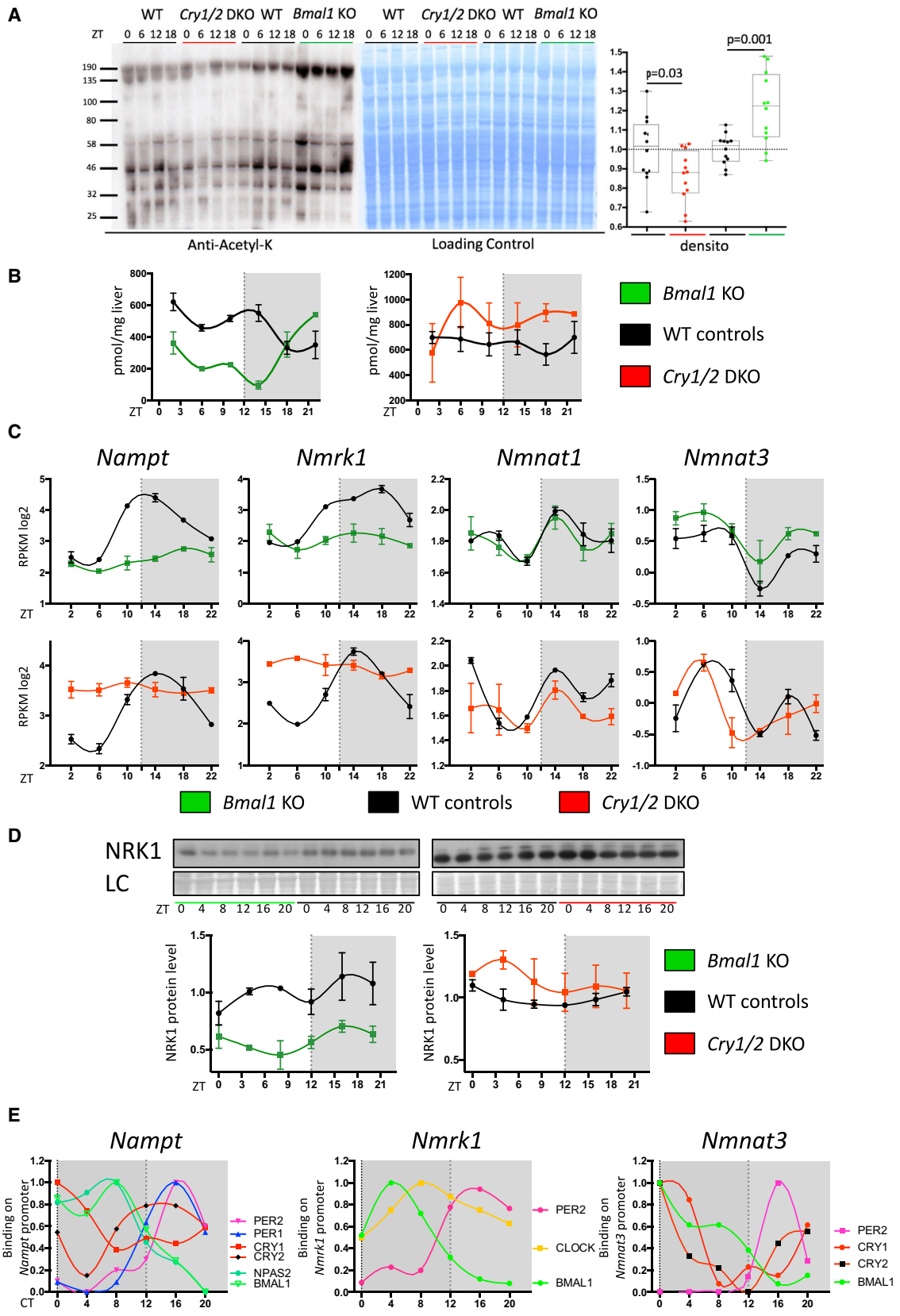

(legend on next page)

Pathways Affected by Circadian Clock-Regulated Acetylation and Links with Metabolism

A search for metabolic pathways enriched in rhythmically acetylated proteins revealed a significant involvement in amino acid and lipid metabolism in addition to citrate (tricarboxylic acid cycle [TCA]) and urea cycles. Moreover, many proteins involved in mitochondrial oxidative phosphorylation, ketogenesis, and ethanol metabolism were also rhythmically acetylated (Figure 5; Figure S4; Table S4). Interestingly, many proteins in these pathways showed deregulated acetylation levels in *Cry1/2* and *Bmal1* KO mice (Figure S5). More specifically, we found that many proteins involved in these pathways presented an increased acetylation level in both KO mice, mainly at ZT18, when rhythmically acetylated mitochondrial proteins showed a minimum level of acetylation in WT mice. Interestingly, acetylation controls several proteins of the TCA cycle. Succinate dehydrogenase A (SDHA) (Cimen et al., 2010; Finley et al., 2011), malate dehydrogenase 2 (MDH2) (Kim et al., 2013), pyruvate dehydrogenase alpha 1 (PDHA) (Fan et al., 2014), and isocitrate dehydrogenase 2 (IDH2) (Yu et al., 2012) are all characterized by reversible acetylation regulated through deacetylation by the deacetylase SIRT3. Except for MDH2, this acetylation leads to enzyme activity inhibition. The global increased acetylation of TCA cycle enzymes in *Cry1/2* and *Bmal1* KO mice (Figure S5) could be a factor explaining the decreased TCA cycle activity that occurs in *Bmal1* KO mice (Peek et al., 2013).

Similar observations were made for the urea cycle, where carbamoyl phosphate synthetase (CPS1) (Ogura et al., 2010), glutamate oxaloacetate transaminase 2 (GOT2) (Yang et al., 2015), and ornithine carbamoyltransferase (OTC) (Hallows et al., 2011; Yu et al., 2009) also possess reversible acetylation as an enzymatic activity regulator. These enzymes also displayed increased acetylation levels in *Cry1/2* and at ZT18 in *Bmal1* KO mice. Most of the enzymes involved in ketogenesis are prone to be regulated by SIRT3 (Dittenhafer-Reed et al., 2015), notably 3-hydroxy-3-methylglutaryl-CoA synthase 2 (HMGCS2) (Shimazu et al., 2010), showing circadian clock-regulated acetylation. The acetyl-CoA synthetase enzymes in the ethanol metabolism pathway are also regulated by SIRT3-dependent deacetylation, which activates their enzymatic activity (Hallows et al., 2006; Schwer et al., 2006). In the same pathway, numerous aldehyde dehydrogenases are known to be deacetylated in a sirtuin-dependent fashion (Lu et al., 2011; Zhao et al., 2014) and show circadian clock-regulated acetylation. Regarding fatty acid oxidation, the enzymes acyl-CoA synthetase I (ACSL1) (Frahm et al., 2011), long-chain acyl CoA dehydrogenase (ACADL) (Hirschey et al., 2010), and enoyl-CoA hydratase/3-hydroxyacyl-CoA (EHHADH) (Zhao et al., 2010) have also been shown to be regulated by acetylation and present altered acetylation in clock-deficient mice. Mitochondrial oxidative phosphorylation protein complexes I to V have been shown to be acetylated (Kim et al., 2006); this acetylation is at least partly under the control of SIRT3 (Rahman et al., 2014). As previously shown for several of these (Cela et al., 2016), rhythmic acetylation of these proteins was found to be subjected to circadian clock regulation. Altogether, these observations suggest that clock-controlled diurnal acetylation could have an effect on global liver metabolism via the regulation of enzymatic activity.

To identify potential effects of the described circadian clock-regulated rhythmic acetylation on metabolism, in addition to the proteomic approach we also performed proton nuclear magnetic resonance (^{1}H-NMR) spectroscopy-based metabolomics on hydrophilic liver tissue extracts from WT and *Bmal1* KO mice. As described in Figures 6 and S6, several reciprocities between levels of metabolites and differential acetylation levels in *Bmal1* KO mice could be found. For instance, in the urea cycle, low levels of arginine and ornithine during the day in *Bmal1* KO animals paralleled the decreased acetylation of ASS1 and ARG1 during this period and the increased acetylation of OTC at ZT18. Although the function of ASS1 and ARG1 acetylation has not yet been described, we could speculate that a decrease in OTC activity because higher acetylation at ZT18 also contributes to this process. In the same pathway, matched low levels of glutamate, α-ketoglutarate, pyruvate, and alanine were also observed during the day, preceded by increased acetylation and inhibition of GLUD1, CPS1, and GOT2 at the end of the night. Several of these metabolites are also part of the imbricate TCA cycle and tie up with the decreased succinate level at day-night transition, when many enzymes presented an increased acetylation level (Figures S5 and S6). In addition to these pathways, we also observed a strong correspondence between low levels of lysine at night-day transition and acetylation of aminoadipate-semialdehyde synthase (AASS), suggesting an uncharacterized link between the acetylation and activity of this enzyme. Finally, several aldehyde dehydrogenases of the ethanol pathway displayed disturbed acetylation in KO mouse liver that could be put alongside a general decrease in acetate levels. We also noted in many cases that quantitative profiles of metabolites are correlated with the profile of NAD^+ level in *Bmal1* KO mice, suggesting a potential role of NAD^+-dependent deacetylase in

Figure 4. Regulation of Global Acetylation and NAD^+ Metabolism by the Circadian Clock

(A) Western blot analysis of global lysine acetylation performed on total protein extract from *Cry1/2* DKO, *Bmal1* KO, and their corresponding WT control mice (left). Naphtol blue black staining of the membrane was used as a loading control (center) and served as a reference for normalization of the quantified values displayed at the right. The average acetylation level was compared between clock-disrupted mice and their controls using Student's t test (n = 12/genotype). Error bars represent min to max.

(B) NAD^+ liver concentrations in *Bmal1* KO (n = 2/time point) and *Cry1/2* DKO mice (n = 2/time point) and their corresponding WT controls (mean ± SEM).

(C) Top: mRNA expression levels of *Nampt*, *Nmrk1*, *Nmnat1*, and *Nmnat3* in *Bmal1* KO mice (green) and their WT littermates (black) under night-restricted feeding conditions. Bottom: the same results in *Cry1/2* DKO (red) mice and their WT controls (black). The data are from Atger et al. (2015); n = 2 for each time point and each genotype). Error bars represent ±SEM.

(D) WB analysis in TE extracts of NRK1 in *Bmal1* KO and *Cry1/2* DKO mice. Quantifications of the blots are displayed below. Naphtol blue black staining of the membranes was used as a loading control and served as a reference for normalization of the quantified values. Error bars represent ±SEM.

(E) Temporal binding of circadian clock core regulators on the *Nampt*, *Nmrk1*, and *Nmnat3* gene promoters. At each time point, for each factor, the averages of all rhythmic bindings are presented. The data are from Koike et al. (2012).

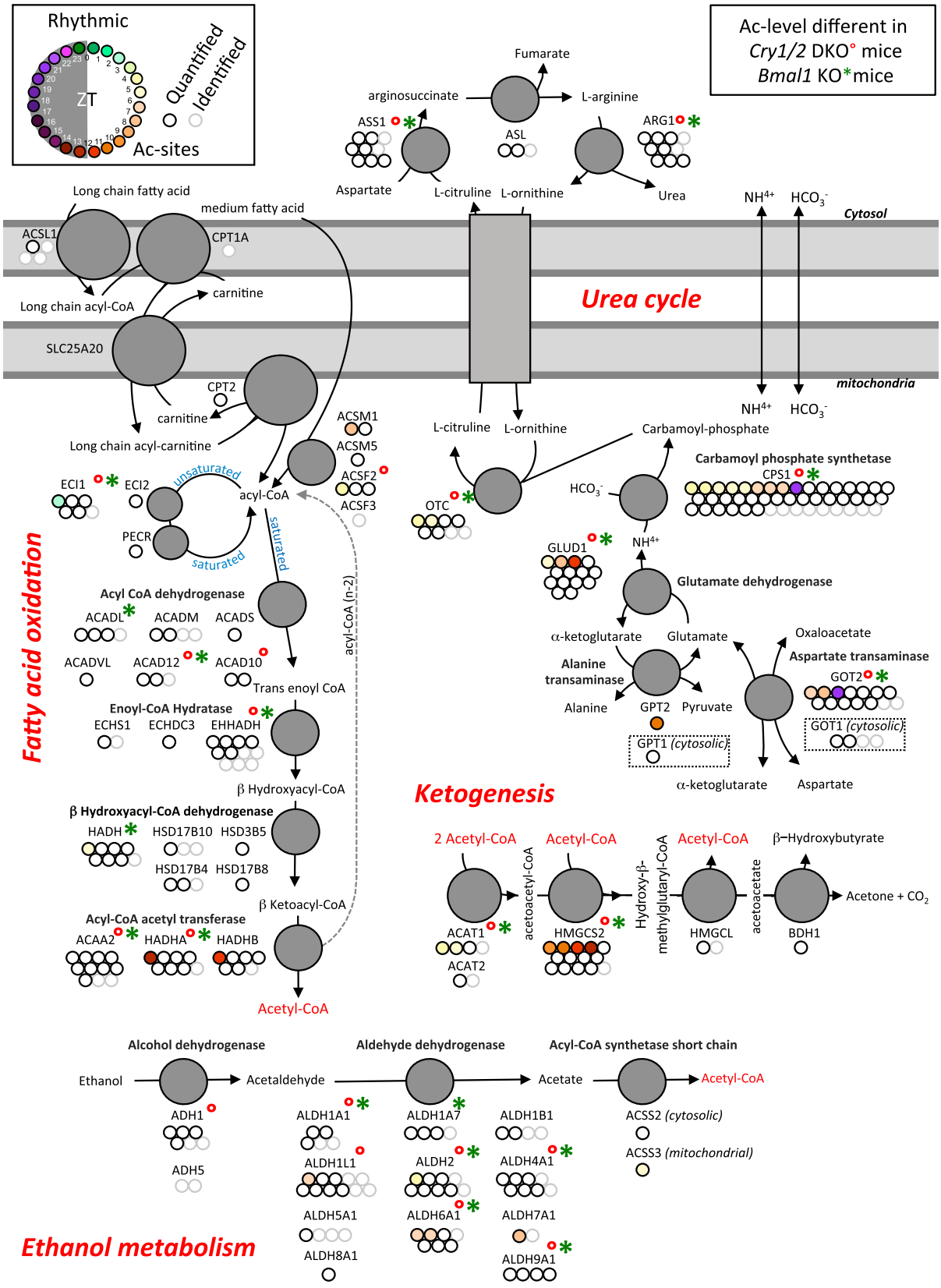

(legend on next page)

the regulation of enzyme activities in the aforementioned metabolic pathways or at least a strong correlation between the two processes (Figures 4B and 6).

DISCUSSION

Although phosphorylation has been considered the major modifier of protein activity and function for a long time, many additional modifications, including acetylation, have emerged as important post-translational modifications (Hirschey and Zhao, 2015). The high-coverage acetylome described here allowed us to gain more insights about diurnal protein acetylation in mouse liver compared with previous work (Masri et al., 2013). In particular, we showed that acetylation of mitochondrial proteins is in the opposite phase compared with the extra-mitochondrial compartments, probably because of the different sirtuins locally expressed within these cell compartments. These rhythmic sirtuin activities, and particularly SIRT3 in mitochondria, are likely the consequence of rhythmic accumulation of NAD^+ in the different cell compartments (Peek et al., 2013). Although regulation of the NAD^+ salvage pathway by the circadian clock through the regulation of *Nampt* expression appeared to be critical during fasting or for cell-autonomous NAD^+ synthesis (Nakahata et al., 2009; Ramsey et al., 2009), this pathway seems to be less critical under normal conditions, where NAD^+ seems to originate mostly from food metabolism. Indeed, the circadian clock controls NAMPT, involved in the synthesis of NAD^+ through the salvage pathway or from the food-contained nicotinamide (NAM), but also NRK1, involved in the synthesis of NAD^+ from NR and NMN (Ratajczak et al., 2016; Figure 7A). The circadian clock therefore regulates most aspects of NAD^+ synthesis in the mouse liver and, by this, enlarges the landscape of interconnection between the circadian clock and sirtuins (Masri and Sassone-Corsi, 2014).

In contrast to the observed maximum acetylation of mitochondrial proteins during the night under fasting conditions because of the more active SIRT3 activity during this period (Peek et al., 2013), we observed, under our night feeding conditions, maximal acetylation of these proteins during the day, mostly as a consequence of the food-dependent increase in acetyl-CoA synthesis (Shi and Tu, 2015). Under these two conditions, this maximal acetylation is correlated with the minimal mitochondrial activity (Neufeld-Cohen et al., 2016; Peek et al., 2013), deacetylation of mitochondrial proteins being key to maintaining proper mitochondrial activity (Hirschey et al., 2010). In addition, feeding rhythms also appear to be important in this pathway because restricted night feeding is able to restore normal rhythmic mitochondrial activity in *Per2* KO animals (Neufeld-Cohen et al., 2016), highlighting the strong interconnection between feeding and the circadian clock in regulating mitochondrial activity. In addition, supplementation strategies designed to improve NAD^+ concentration protect against metabolic diseases, neurodegenerative disorders, and age-related physiological decline in mammals (Cantó et al., 2015). The key role of the circadian clock in regulating NAD^+ synthesis suggests that timing of supplementation should also be taken into account as an important aspect of this strategy.

Our study also shows the key role of the circadian clock in the metabolism of vitamin B3, nicotinic acid (NA) constituting another source of NAD^+. Interestingly, circulating levels of several vitamins, like vitamins A, B9, B12, D, E, and K, showed a diurnal rhythm in mammals (Hutchins and Ball, 1983; Piccione et al., 2004), but the role of the circadian clock in these rhythms has not yet been established. One exception is vitamin B6, for which a clear role of the clock has been demonstrated through the regulation of pyridoxal kinase (*Pdxk*) by the circadian clock-regulated proline acidic amino acid-rich basic leucine zipper (PARbZip) transcription factors (Gachon et al., 2004). All of these elements suggest that the circadian clock, in addition to its role in macronutrient metabolism, also plays a crucial role in micronutrient and vitamin metabolism. Given the broad effect of these circadian clock-regulated vitamins in general metabolism, in particular neurotransmitter synthesis for vitamin B6 (Gachon et al., 2004) and mitochondrial activity for vitamin B3 (Menzies et al., 2016), this pathway likely contributes to the metabolic deficiency observed in circadian clock-deficient animals.

Although acetylation is currently the most described modification of lysine residues by acylation, lysine can also alternatively be formylated, methylated, propionylated, butyrylated, crotonylated, malonylated, succinylated, glutarylated, or myristoylated (Choudhary et al., 2014). Sirtuins are also involved in the deacylation of these lysine modifications, playing an important role in the regulation of metabolism. SIRT5, for instance, has recently been shown to regulate glycolysis through reversible malonylation (Nishida et al., 2015), the urea cycle through deglutarylation (Tan et al., 2014), and ketogenesis as well as other metabolic pathways through desuccinylation (Park et al., 2013; Rardin et al., 2013a). Interestingly, these activities are also NAD^+-dependent and, as a result, potentially subjected to circadian clock regulation. Using antibodies specific to malonylated and succinylated lysine, we also showed that malonylation was increased in the liver of *Bmal1* KO mice, whereas succinylation was decreased in *Cry1/2* DKO mice and increased in *Bmal1* KO mice (Figures 7B and 7C), in accordance with NAD^+ levels in these animals. These additional findings suggest that the circadian clock, in addition to its key role in the regulation of transcription, is also able to regulate key metabolic function through post-translational regulation events, including acetylation, and probably other metabolism-related lysine acylations.

Figure 5. Metabolic Pathways Affected by Rhythmic Acetylation

Rhythmic protein acetylations and their regulation by the circadian clock for fatty acid oxydation, urea cycle, ketogenesis, and ethanol metabolism. Each dot represents a unique acetylation site within the protein of interest. Grey and black dots represent non-rhythmic identified and quantified acetylation sites, respectively, whereas phases of maximum acetylation levels for rhythmic acetylation sites are color-coded. Superscripted red dots and green asterisks indicate protein acetylation levels significantly different in *Cry1/2* DKO and *Bmal1* KO mice, respectively.

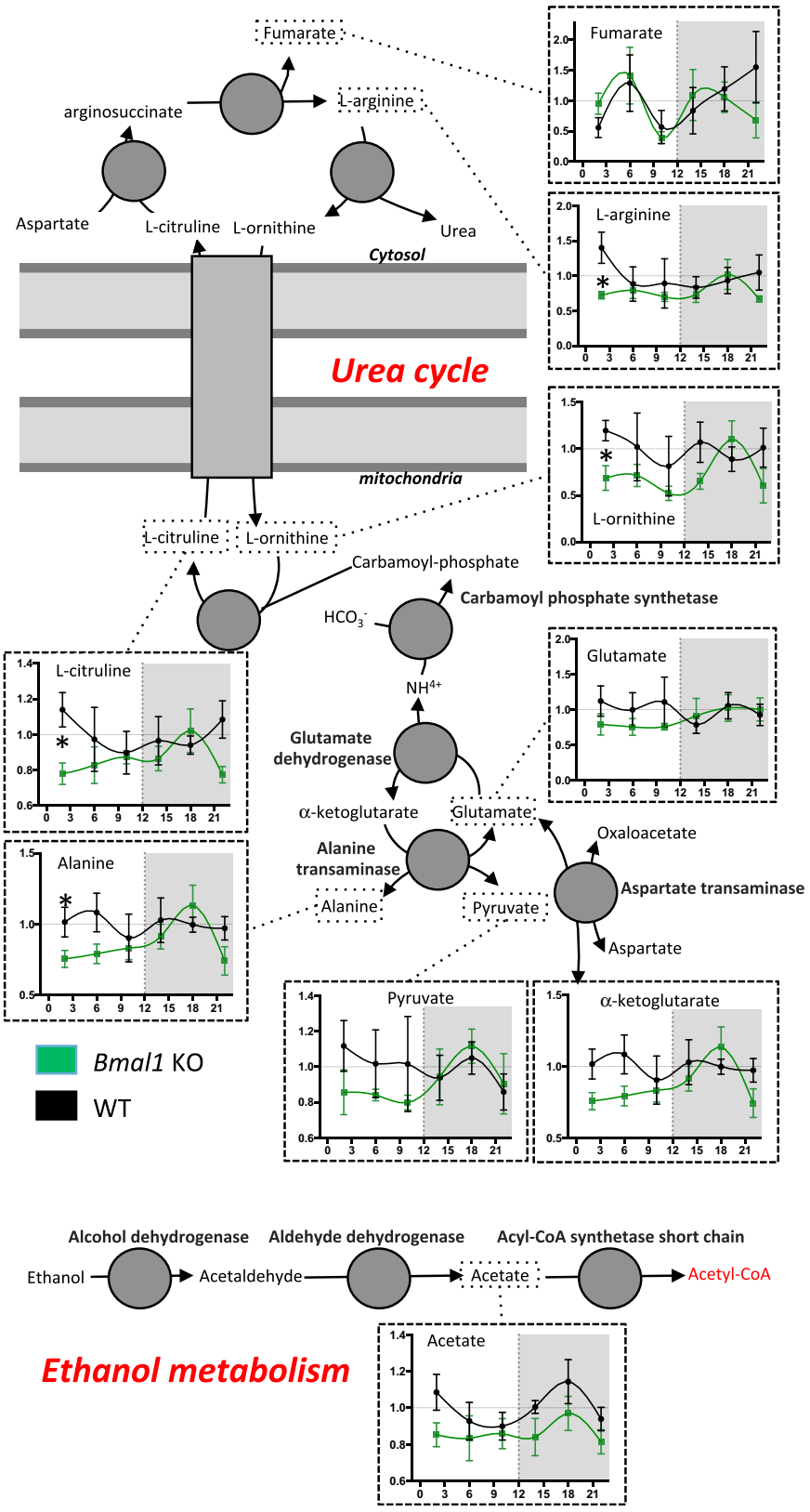

Figure 6. Impact of Rhythmic Acetylation on Metabolite Levels

Liver temporal profiles of metabolites in *Bmal1* KO (green lines) and WT littermates (black lines). Data (mean ± SEM) are expressed relative to the temporal mean of WT values. The analysis is related to key metabolites of the urea cycle, ketogenesis, and ethanol metabolism. Student's t test was performed to compare the average level of metabolite at every time point between different genotypes (n = 4). *p < 0.05 between *Bmal1* KO and WT mice.

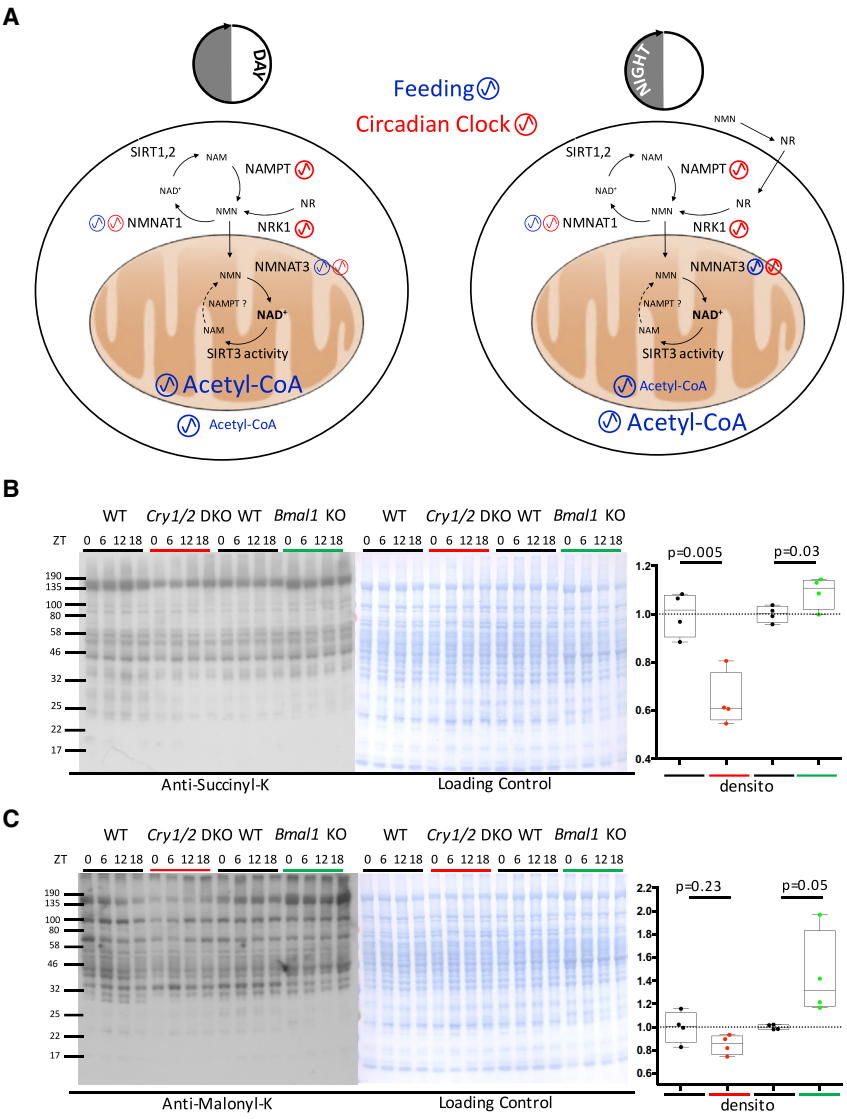

Figure 7. Interconnection between Feeding and Circadian Rhythms in Regulating NAD$^+$ Synthesis and Circadian Clock Disruption Effects on Lysine Succinylation and Malonylation

(A) Rhythmic feeding effect (blue) versus the circadian clock (red) on key components implicated in acetyl-CoA-dependent acetylation and the regulation NAD$^+$ synthesis during the day (fasting phase) and night (feeding phase).

(B and C) Western blot analysis of global lysine succinylation (B) and malonylation (C) performed on total protein extract from *Cry1/2* DKO, *Bmal1* KO, and their corresponding WT control mice (left). Naphtol blue black staining of the membrane was used as a loading control (center) and served as a reference for normalization of the quantified values displayed at the right. Average acetylation levels were compared between clock-disrupted mice and their controls using Student's t test (n = 4). Error bars represent min to max.

EXPERIMENTAL PROCEDURES

Animal Experiments

Animal studies were conducted in accordance with the regulations of the veterinary office of the Canton of Vaud. *Cry1/2* DKO mice in the C57BL/6J genetic background (Bur et al., 2009) and *Bmal1* KO mice (Jouffe et al., 2013) have been described previously. Mice had free access to food and water in 12-hr light/12-hr dark cycles under standard animal housing conditions. However, unless indicated otherwise, in all experiments animals were fed only at night, starting 4 days before the experiment. SILAC mice, generated according to a standard procedure (Krüger et al., 2008), have been described previously (Mauvoisin et al., 2014).

Total and Nuclear Protein Extraction

TE and NE protein extracts were generated as described previously (Wang et al., 2017). The detailed procedure can be found in the Supplemental Experimental Procedures.

Analysis of Acetylation by RP-LC MS/MS

The detailed procedure for the RP-LC MS/MS analysis of lysine-acetylated enriched peptides can be found in the Supplemental Experimental Procedures.

The accession numbers for the mass spectrometry proteomic data reported in this paper were deposited in the ProteomeXchange Consortium via the PRIDE partner repository: PXD005317 and PXD005310 for TE and NE, respectively.

Annotation of Protein Localization

We used UNIPROT (UniProt Consortium, 2015) and COMPARTMENT (Binder et al., 2014) to annotate protein localization (i.e., nuclear, shuttling, cytoplasmic, or mitochondrial), for TE and NE.

Analysis of Rhythmicity

We assessed the rhythmicity in temporal accumulations of acetylated sites normalized by corresponding protein levels using harmonic regression as described previously (Mauvoisin et al., 2014).

KEGG Pathway Enrichment Analysis

The Kyoto Encyclopedia of Genes and Genomes (KEGG) pathway enrichment for quantified proteins was performed using the Database of Annotation, Visualization and Integrated Discovery (DAVID) Bioinformatics Resources 6.8. at https://david.ncifcrf.gov/home.jsp (Huang et al., 2009).

Western Blotting

20 μg of total liver protein was used for western blotting according to standard procedures. Densitometry analyses of the blots were performed using the ImageJ software. Naphtol blue black staining of the membranes was used as a loading control and served as a reference for normalization of the quantified values. References for antibodies used in this paper can be found in the Supplemental Experimental Procedures.

NAD$^+$ Concentration

Liver NAD$^+$ concentration was assessed with the EnzyChrom NAD/NADH Assay Kit (BioAssay Systems) on ~25 mg of liver tissue and according to the manufacturer's instructions.

^{1}H NMR Spectroscopic Analysis of Liver Metabonome

The detailed procedure for ^{1}H NMR metabonomic analysis of liver extracts can be found in the Supplemental Experimental Procedures.

ACCESSION NUMBERS

The accession numbers for the mass spectrometry proteomic data for TE and NE, respectively, reported in this paper are ProteomeXchange Consortium via the PRIDE partner repository: PXD005317 and PXD005310.

SUPPLEMENTAL INFORMATION

Supplemental Information includes Supplemental Experimental Procedures, six figures, and four tables and can be found with this article online at http://dx.doi.org/10.1016/j.celrep.2017.07.065.

AUTHOR CONTRIBUTIONS

Conceptualization, D.M. and F.G.; Formal Analysis, D.M., J.W., F.N., and F.G.; Investigation, D.M., F.A., E.M., J.R., and C.C.; Proteomics Data Acquisition and Curation, L.D., A.N.G., and M.K.; Metabolomics Data Acquisition and Curation, L.D.S., I.M., S.C., and F.P.M.; Visualization, D.M. and J.W.; Writing – Original Draft, D.M. and F.G.; Writing – Review & Editing, D.M., F.A., L.D., A.N.G., J.W., E.M., L.D.S., I.M., S.C., F.P.M., J.R., C.C., M.K., F.N., and F.G.; Supervision, F.N. and F.G.; Funding Acquisition, F.N. and F.G.

ACKNOWLEDGMENTS

This research was supported by the Swiss National Science Foundation (through individual research grants 31003A-153340 and 310030-173079 to F.N.), the Ecole Polytechnique Fédérale de Lausanne, the Novartis Foundation for Medical-Biological Research (16C213 to F.N.), the European Research Council (through individual starting grant ERC-2010-StG-260988 to F.G.), and the Leenaards Foundation (to F.G. and F.N.). We thank Philipp Gut for positive insightful discussions and comments. The authors thank Prof. Gijsbertus van der Horst (Erasmus University Medical Center, Rotterdam, the Netherlands) for providing *Cry1/2* DKO mice. D.M., F.A., L.D., A.N.G., E.M., L.D.S., I.M., F.P.M., J.R., C.C., M.K., and F.G. are employees of the Nestlé Institute of Health Sciences S.A.

Received: March 8, 2017
Revised: June 12, 2017
Accepted: July 24, 2017
Published: August 15, 2017

REFERENCES

Asher, G., Gatfield, D., Stratmann, M., Reinke, H., Dibner, C., Kreppel, F., Mostoslavsky, R., Alt, F.W., and Schibler, U. (2008). SIRT1 regulates circadian clock gene expression through PER2 deacetylation. Cell *134*, 317–328.

Atger, F., Gobet, C., Marquis, J., Martin, E., Wang, J., Weger, B., Lefebvre, G., Descombes, P., Naef, F., and Gachon, F. (2015). Circadian and feeding rhythms differentially affect rhythmic mRNA transcription and translation in mouse liver. Proc. Natl. Acad. Sci. USA *112*, E6579–E6588.

Binder, J.X., Pletscher-Frankild, S., Tsafou, K., Stolte, C., O'Donoghue, S.I., Schneider, R., and Jensen, L.J. (2014). COMPARTMENTS: unification and visualization of protein subcellular localization evidence. Database (Oxford) *2014*, bau012.

Bur, I.M., Cohen-Solal, A.M., Carmignac, D., Abecassis, P.-Y., Chauvet, N., Martin, A.O., van der Horst, G.T.J., Robinson, I.C.A.F., Maurel, P., Mollard, P., and Bonnefont, X. (2009). The circadian clock components CRY1 and CRY2 are necessary to sustain sex dimorphism in mouse liver metabolism. J. Biol. Chem. *284*, 9066–9073.

Cambronne, X.A., Stewart, M.L., Kim, D., Jones-Brunette, A.M., Morgan, R.K., Farrens, D.L., Cohen, M.S., and Goodman, R.H. (2016). Biosensor reveals multiple sources for mitochondrial NAD^+. Science *352*, 1474–1477.

Cantó, C., Menzies, K.J., and Auwerx, J. (2015). $NAD(^+)$ Metabolism and the Control of Energy Homeostasis: A Balancing Act between Mitochondria and the Nucleus. Cell Metab. *22*, 31–53.

Cela, O., Scrima, R., Pazienza, V., Merla, G., Benegiamo, G., Augello, B., Fugetto, S., Menga, M., Rubino, R., Fuhr, L., et al. (2016). Clock genes-dependent acetylation of complex I sets rhythmic activity of mitochondrial OxPhos. Biochim. Biophys. Acta *1863*, 596–606.

Chavan, R., Feillet, C., Costa, S.S.F., Delorme, J.E., Okabe, T., Ripperger, J.A., and Albrecht, U. (2016). Liver-derived ketone bodies are necessary for food anticipation. Nat. Commun. *7*, 10580.

Chen, Y., Zhang, J., Lin, Y., Lei, Q., Guan, K.L., Zhao, S., and Xiong, Y. (2011). Tumour suppressor SIRT3 deacetylates and activates manganese superoxide dismutase to scavenge ROS. EMBO Rep. *12*, 534–541.

Choudhary, C., Kumar, C., Gnad, F., Nielsen, M.L., Rehman, M., Walther, T.C., Olsen, J.V., and Mann, M. (2009). Lysine acetylation targets protein complexes and co-regulates major cellular functions. Science *325*, 834–840.

Choudhary, C., Weinert, B.T., Nishida, Y., Verdin, E., and Mann, M. (2014). The growing landscape of lysine acetylation links metabolism and cell signalling. Nat. Rev. Mol. Cell Biol. *15*, 536–550.

Cimen, H., Han, M.-J., Yang, Y., Tong, Q., Koc, H., and Koc, E.C. (2010). Regulation of succinate dehydrogenase activity by SIRT3 in mammalian mitochondria. Biochemistry *49*, 304–311.

Crane, B.R., and Young, M.W. (2014). Interactive features of proteins composing eukaryotic circadian clocks. Annu. Rev. Biochem. *83*, 191–219.

Dittenhafer-Reed, K.E., Richards, A.L., Fan, J., Smallegan, M.J., Fotuhi Siahpirani, A., Kemmerer, Z.A., Prolla, T.A., Roy, S., Coon, J.J., and Denu, J.M. (2015). SIRT3 mediates multi-tissue coupling for metabolic fuel switching. Cell Metab. *21*, 637–646.

Drew, J.E., Farquharson, A.J., Horgan, G.W., and Williams, L.M. (2016). Tissue-specific regulation of sirtuin and nicotinamide adenine dinucleotide biosynthetic pathways identified in C57Bl/6 mice in response to high-fat feeding. J. Nutr. Biochem. *37*, 20–29.

Du, J., Zhou, Y., Su, X., Yu, J.J., Khan, S., Jiang, H., Kim, J., Woo, J., Kim, J.H., Choi, B.H., et al. (2011). Sirt5 is a NAD-dependent protein lysine demalonylase and desuccinylase. Science *334*, 806–809.

Fan, J., Shan, C., Kang, H.-B., Elf, S., Xie, J., Tucker, M., Gu, T.-L., Aguiar, M., Lonning, S., Chen, H., et al. (2014). Tyr phosphorylation of PDP1 toggles recruitment between ACAT1 and SIRT3 to regulate the pyruvate dehydrogenase complex. Mol. Cell *53*, 534–548.

Finley, L.W.S., Haas, W., Desquiret-Dumas, V., Wallace, D.C., Procaccio, V., Gygi, S.P., and Haigis, M.C. (2011). Succinate dehydrogenase is a direct target of sirtuin 3 deacetylase activity. PLoS ONE *6*, e23295.

Frahm, J.L., Li, L.O., Grevengoed, T.J., and Coleman, R.A. (2011). Phosphorylation and Acetylation of Acyl-CoA Synthetase- I. J. Proteomics Bioinform. *4*, 129–137.

Gachon, F., Fonjallaz, P., Damiola, F., Gos, P., Kodama, T., Zakany, J., Duboule, D., Petit, B., Tafti, M., and Schibler, U. (2004). The loss of circadian PAR bZip transcription factors results in epilepsy. Genes Dev. *18*, 1397–1412.

Gerhart-Hines, Z., and Lazar, M.A. (2015). Circadian metabolism in the light of evolution. Endocr. Rev. *36*, 289–304.

Hallows, W.C., Lee, S., and Denu, J.M. (2006). Sirtuins deacetylate and activate mammalian acetyl-CoA synthetases. Proc. Natl. Acad. Sci. USA *103*, 10230–10235.

Hallows, W.C., Yu, W., Smith, B.C., Devries, M.K., Ellinger, J.J., Someya, S., Shortreed, M.R., Prolla, T., Markley, J.L., Smith, L.M., et al. (2011). Sirt3 promotes the urea cycle and fatty acid oxidation during dietary restriction. Mol. Cell *41*, 139–149.

Hebert, A.S., Dittenhafer-Reed, K.E., Yu, W., Bailey, D.J., Selen, E.S., Boersma, M.D., Carson, J.J., Tonelli, M., Balloon, A.J., Higbee, A.J., et al. (2013). Calorie restriction and SIRT3 trigger global reprogramming of the mitochondrial protein acetylome. Mol. Cell *49*, 186–199.

Hirschey, M.D., and Zhao, Y. (2015). Metabolic Regulation by Lysine Malonylation, Succinylation, and Glutarylation. Mol. Cell. Proteomics *14*, 2308–2315.

Hirschey, M.D., Shimazu, T., Goetzman, E., Jing, E., Schwer, B., Lombard, D.B., Grueter, C.A., Harris, C., Biddinger, S., Ilkayeva, O.R., et al. (2010).

SIRT3 regulates mitochondrial fatty-acid oxidation by reversible enzyme deacetylation. Nature *464*, 121–125.

Huang, W., Sherman, B.T., and Lempicki, R.A. (2009). Systematic and integrative analysis of large gene lists using DAVID bioinformatics resources. Nat. Protoc. *4*, 44–57.

Hutchins, D.A., and Ball, P.E. (1983). Circadian rhythms of folate and vitamin $B_{(12)}$ concentration in relation to convulsive thresholds of mice. Neurochem. Int. *5*, 421–427.

Jouffe, C., Cretenet, G., Symul, L., Martin, E., Atger, F., Naef, F., and Gachon, F. (2013). The circadian clock coordinates ribosome biogenesis. PLoS Biol. *11*, e1001455.

Jukarainen, S., Heinonen, S., Rämö, J.T., Rinnankoski-Tuikka, R., Rappou, E., Tummers, M., Muniandy, M., Hakkarainen, A., Lundbom, J., Lundbom, N., et al. (2016). Obesity Is Associated With Low NAD(+)/SIRT Pathway Expression in Adipose Tissue of BMI-Discordant Monozygotic Twins. J. Clin. Endocrinol. Metab. *101*, 275–283.

Kim, S.C., Sprung, R., Chen, Y., Xu, Y., Ball, H., Pei, J., Cheng, T., Kho, Y., Xiao, H., Xiao, L., et al. (2006). Substrate and functional diversity of lysine acetylation revealed by a proteomics survey. Mol. Cell *23*, 607–618.

Kim, E.-J., Kho, J.-H., Kang, M.-R., and Um, S.-J. (2007). Active regulator of SIRT1 cooperates with SIRT1 and facilitates suppression of p53 activity. Mol. Cell *28*, 277–290.

Kim, E.Y., Han, B.S., Kim, W.K., Lee, S.C., and Bae, K.-H. (2013). Acceleration of adipogenic differentiation via acetylation of malate dehydrogenase 2. Biochem. Biophys. Res. Commun. *441*, 77–82.

Koike, N., Yoo, S.-H., Huang, H.-C., Kumar, V., Lee, C., Kim, T.-K., and Takahashi, J.S. (2012). Transcriptional architecture and chromatin landscape of the core circadian clock in mammals. Science *338*, 349–354.

Krüger, M., Moser, M., Ussar, S., Thievessen, I., Luber, C.A., Forner, F., Schmidt, S., Zanivan, S., Fässler, R., and Mann, M. (2008). SILAC mouse for quantitative proteomics uncovers kindlin-3 as an essential factor for red blood cell function. Cell *134*, 353–364.

Lombard, D.B., Alt, F.W., Cheng, H.-L., Bunkenborg, J., Streeper, R.S., Mostoslavsky, R., Kim, J., Yancopoulos, G., Valenzuela, D., Murphy, A., et al. (2007). Mammalian Sir2 homolog SIRT3 regulates global mitochondrial lysine acetylation. Mol. Cell. Biol. *27*, 8807–8814.

Lu, Z., Bourdi, M., Li, J.H., Aponte, A.M., Chen, Y., Lombard, D.B., Gucek, M., Pohl, L.R., and Sack, M.N. (2011). SIRT3-dependent deacetylation exacerbates acetaminophen hepatotoxicity. EMBO Rep. *12*, 840–846.

Lundby, A., Lage, K., Weinert, B.T., Bekker-Jensen, D.B., Secher, A., Skovgaard, T., Kelstrup, C.D., Dmytriyev, A., Choudhary, C., Lundby, C., and Olsen, J.V. (2012). Proteomic analysis of lysine acetylation sites in rat tissues reveals organ specificity and subcellular patterns. Cell Rep. *2*, 419–431.

Masri, S., and Sassone-Corsi, P. (2014). Sirtuins and the circadian clock: bridging chromatin and metabolism. Sci. Signal. *7*, re6.

Masri, S., Patel, V.R., Eckel-Mahan, K.L., Peleg, S., Forne, I., Ladurner, A.G., Baldi, P., Imhof, A., and Sassone-Corsi, P. (2013). Circadian acetylome reveals regulation of mitochondrial metabolic pathways. Proc. Natl. Acad. Sci. USA *110*, 3339–3344.

Mathias, R.A., Greco, T.M., Oberstein, A., Budayeva, H.G., Chakrabarti, R., Rowland, E.A., Kang, Y., Shenk, T., and Cristea, I.M. (2014). Sirtuin 4 is a lipoamidase regulating pyruvate dehydrogenase complex activity. Cell *159*, 1615–1625.

Mauvoisin, D., Wang, J., Jouffe, C., Martin, E., Atger, F., Waridel, P., Quadroni, M., Gachon, F., and Naef, F. (2014). Circadian clock-dependent and -independent rhythmic proteomes implement distinct diurnal functions in mouse liver. Proc. Natl. Acad. Sci. USA *111*, 167–172.

Mauvoisin, D., Dayon, L., Gachon, F., and Kussmann, M. (2015). Proteomics and circadian rhythms: it's all about signaling!. Proteomics *15*, 310–317.

Menzies, K.J., Zhang, H., Katsyuba, E., and Auwerx, J. (2016). Protein acetylation in metabolism - metabolites and cofactors. Nat. Rev. Endocrinol. *12*, 43–60.

Monaghan, R.M., and Whitmarsh, A.J. (2015). Mitochondrial Proteins Moonlighting in the Nucleus. Trends Biochem. Sci. *40*, 728–735.

Mori, V., Amici, A., Mazzola, F., Di Stefano, M., Conforti, L., Magni, G., Ruggieri, S., Raffaelli, N., and Orsomando, G. (2014). Metabolic profiling of alternative NAD biosynthetic routes in mouse tissues. PLoS ONE *9*, e113939.

Nakahata, Y., Sahar, S., Astarita, G., Kaluzova, M., and Sassone-Corsi, P. (2009). Circadian control of the NAD^+ salvage pathway by CLOCK-SIRT1. Science *324*, 654–657.

Neufeld-Cohen, A., Robles, M.S., Aviram, R., Manella, G., Adamovich, Y., Ladeuix, B., Nir, D., Rousso-Noori, L., Kuperman, Y., Golik, M., et al. (2016). Circadian control of oscillations in mitochondrial rate-limiting enzymes and nutrient utilization by PERIOD proteins. Proc. Natl. Acad. Sci. USA *113*, E1673–E1682.

Nishida, Y., Rardin, M.J., Carrico, C., He, W., Sahu, A.K., Gut, P., Najjar, R., Fitch, M., Hellerstein, M., Gibson, B.W., and Verdin, E. (2015). SIRT5 Regulates both Cytosolic and Mitochondrial Protein Malonylation with Glycolysis as a Major Target. Mol. Cell *59*, 321–332.

Ogura, M., Nakamura, Y., Tanaka, D., Zhuang, X., Fujita, Y., Obara, A., Hamasaki, A., Hosokawa, M., and Inagaki, N. (2010). Overexpression of SIRT5 confirms its involvement in deacetylation and activation of carbamoyl phosphate synthetase 1. Biochem. Biophys. Res. Commun. *393*, 73–78.

Park, J., Chen, Y., Tishkoff, D.X., Peng, C., Tan, M., Dai, L., Xie, Z., Zhang, Y., Zwaans, B.M.M., Skinner, M.E., et al. (2013). SIRT5-mediated lysine desuccinylation impacts diverse metabolic pathways. Mol. Cell *50*, 919–930.

Peek, C.B., Affinati, A.H., Ramsey, K.M., Kuo, H.-Y., Yu, W., Sena, L.A., Ilkayeva, O., Marcheva, B., Kobayashi, Y., Omura, C., et al. (2013). Circadian clock NAD^+ cycle drives mitochondrial oxidative metabolism in mice. Science *342*, 1243417.

Piccione, G., Assenza, A., Grasso, F., and Caola, G. (2004). Daily rhythm of circulating fat soluble vitamin concentration (A, D, E and K) in the horse. J. Circadian Rhythms *2*, 3.

Rahman, M., Nirala, N.K., Singh, A., Zhu, L.J., Taguchi, K., Bamba, T., Fukusaki, E., Shaw, L.M., Lambright, D.G., Acharya, J.K., and Acharya, U.R. (2014). *Drosophila* Sirt2/mammalian SIRT3 deacetylates ATP synthase β and regulates complex V activity. J. Cell Biol. *206*, 289–305.

Ramsey, K.M., Yoshino, J., Brace, C.S., Abrassart, D., Kobayashi, Y., Marcheva, B., Hong, H.-K., Chong, J.L., Buhr, E.D., Lee, C., et al. (2009). Circadian clock feedback cycle through NAMPT-mediated NAD^+ biosynthesis. Science *324*, 651–654.

Rardin, M.J., He, W., Nishida, Y., Newman, J.C., Carrico, C., Danielson, S.R., Guo, A., Gut, P., Sahu, A.K., Li, B., et al. (2013a). SIRT5 regulates the mitochondrial lysine succinylome and metabolic networks. Cell Metab. *18*, 920–933.

Rardin, M.J., Newman, J.C., Held, J.M., Cusack, M.P., Sorensen, D.J., Li, B., Schilling, B., Mooney, S.D., Kahn, C.R., Verdin, E., and Gibson, B.W. (2013b). Label-free quantitative proteomics of the lysine acetylome in mitochondria identifies substrates of SIRT3 in metabolic pathways. Proc. Natl. Acad. Sci. USA *110*, 6601–6606.

Ratajczak, J., Joffraud, M., Trammell, S.A.J., Ras, R., Canela, N., Boutant, M., Kulkarni, S.S., Rodrigues, M., Redpath, P., Migaud, M.E., et al. (2016). NRK1 controls nicotinamide mononucleotide and nicotinamide riboside metabolism in mammalian cells. Nat. Commun. *7*, 13103.

Robles, M.S., Cox, J., and Mann, M. (2014). In-vivo quantitative proteomics reveals a key contribution of post-transcriptional mechanisms to the circadian regulation of liver metabolism. PLoS Genet. *10*, e1004047.

Robles, M.S., Humphrey, S.J., and Mann, M. (2017). Phosphorylation Is a Central Mechanism for Circadian Control of Metabolism and Physiology. Cell Metab. *25*, 118–127.

Schwer, B., Bunkenborg, J., Verdin, R.O., Andersen, J.S., and Verdin, E. (2006). Reversible lysine acetylation controls the activity of the mitochondrial enzyme acetyl-CoA synthetase 2. Proc. Natl. Acad. Sci. USA *103*, 10224–10229.

Schwer, B., Eckersdorff, M., Li, Y., Silva, J.C., Fermin, D., Kurtev, M.V., Giallourakis, C., Comb, M.J., Alt, F.W., and Lombard, D.B. (2009). Calorie restriction alters mitochondrial protein acetylation. Aging Cell *8*, 604–606.

Shi, L., and Tu, B.P. (2015). Acetyl-CoA and the regulation of metabolism: mechanisms and consequences. Curr. Opin. Cell Biol. *33*, 125–131.

Shimazu, T., Hirschey, M.D., Hua, L., Dittenhafer-Reed, K.E., Schwer, B., Lombard, D.B., Li, Y., Bunkenborg, J., Alt, F.W., Denu, J.M., et al. (2010). SIRT3 deacetylates mitochondrial 3-hydroxy-3-methylglutaryl CoA synthase 2 and regulates ketone body production. Cell Metab. *12*, 654–661.

Siess, E.A., Brocks, D.G., and Wieland, O.H. (1978). Distribution of metabolites between the cytosolic and mitochondrial compartments of hepatocytes isolated from fed rats. Hoppe Seylers Z. Physiol. Chem. *359*, 785–798.

Smith, K.T., and Workman, J.L. (2009). Introducing the acetylome. Nat. Biotechnol. *27*, 917–919.

Still, A.J., Floyd, B.J., Hebert, A.S., Bingman, C.A., Carson, J.J., Gunderson, D.R., Dolan, B.K., Grimsrud, P.A., Dittenhafer-Reed, K.E., Stapleton, D.S., et al. (2013). Quantification of mitochondrial acetylation dynamics highlights prominent sites of metabolic regulation. J. Biol. Chem. *288*, 26209–26219.

Storch, K.-F., Paz, C., Signorovitch, J., Raviola, E., Pawlyk, B., Li, T., and Weitz, C.J. (2007). Intrinsic circadian clock of the mammalian retina: importance for retinal processing of visual information. Cell *130*, 730–741.

Tan, M., Peng, C., Anderson, K.A., Chhoy, P., Xie, Z., Dai, L., Park, J., Chen, Y., Huang, H., Zhang, Y., et al. (2014). Lysine glutarylation is a protein posttranslational modification regulated by SIRT5. Cell Metab. *19*, 605–617.

UniProt Consortium (2015). UniProt: a hub for protein information. Nucleic Acids Res. *43*, D204–D212.

van der Horst, G.T.J., Muijtjens, M., Kobayashi, K., Takano, R., Kanno, S., Takao, M., de Wit, J., Verkerk, A., Eker, A.P.M., van Leenen, D., et al. (1999). Mammalian Cry1 and Cry2 are essential for maintenance of circadian rhythms. Nature *398*, 627–630.

Verdin, E., Hirschey, M.D., Finley, L.W.S., and Haigis, M.C. (2010). Sirtuin regulation of mitochondria: energy production, apoptosis, and signaling. Trends Biochem. Sci. *35*, 669–675.

Wang, J., Mauvoisin, D., Martin, E., Atger, F., Galindo, A.N., Dayon, L., Sizzano, F., Palini, A., Kussmann, M., Waridel, P., et al. (2017). Nuclear Proteomics Uncovers Diurnal Regulatory Landscapes in Mouse Liver. Cell Metab. *25*, 102–117.

Weinert, B.T., Moustafa, T., Iesmantavicius, V., Zechner, R., and Choudhary, C. (2015). Analysis of acetylation stoichiometry suggests that SIRT3 repairs nonenzymatic acetylation lesions. EMBO J. *34*, 2620–2632.

Wellen, K.E., and Thompson, C.B. (2012). A two-way street: reciprocal regulation of metabolism and signalling. Nat. Rev. Mol. Cell Biol. *13*, 270–276.

Woller, A., Duez, H., Staels, B., and Lefranc, M. (2016). A Mathematical Model of the Liver Circadian Clock Linking Feeding and Fasting Cycles to Clock Function. Cell Rep. *17*, 1087–1097.

Wu, R., Haas, W., Dephoure, N., Huttlin, E.L., Zhai, B., Sowa, M.E., and Gygi, S.P. (2011). A large-scale method to measure absolute protein phosphorylation stoichiometries. Nat. Methods *8*, 677–683.

Yang, L., Vaitheesvaran, B., Hartil, K., Robinson, A.J., Hoopmann, M.R., Eng, J.K., Kurland, I.J., and Bruce, J.E. (2011). The fasted/fed mouse metabolic acetylome: N6-acetylation differences suggest acetylation coordinates organ-specific fuel switching. J. Proteome Res. *10*, 4134–4149.

Yang, H., Zhou, L., Shi, Q., Zhao, Y., Lin, H., Zhang, M., Zhao, S., Yang, Y., Ling, Z.-Q., Guan, K.-L., et al. (2015). SIRT3-dependent GOT2 acetylation status affects the malate-aspartate NADH shuttle activity and pancreatic tumor growth. EMBO J. *34*, 1110–1125.

Yu, W., Lin, Y., Yao, J., Huang, W., Lei, Q., Xiong, Y., Zhao, S., and Guan, K.-L. (2009). Lysine 88 acetylation negatively regulates ornithine carbamoyltransferase activity in response to nutrient signals. J. Biol. Chem. *284*, 13669–13675.

Yu, W., Dittenhafer-Reed, K.E., and Denu, J.M. (2012). SIRT3 protein deacetylates isocitrate dehydrogenase 2 (IDH2) and regulates mitochondrial redox status. J. Biol. Chem. *287*, 14078–14086.

Zhao, S., Xu, W., Jiang, W., Yu, W., Lin, Y., Zhang, T., Yao, J., Zhou, L., Zeng, Y., Li, H., et al. (2010). Regulation of cellular metabolism by protein lysine acetylation. Science *327*, 1000–1004.

Zhao, D., Mo, Y., Li, M.-T., Zou, S.-W., Cheng, Z.-L., Sun, Y.-P., Xiong, Y., Guan, K.-L., and Lei, Q.-Y. (2014). NOTCH-induced aldehyde dehydrogenase 1A1 deacetylation promotes breast cancer stem cells. J. Clin. Invest. *124*, 5453–5465.

Cell Reports, Volume *20*

Supplemental Information

Circadian and Feeding Rhythms Orchestrate the Diurnal Liver Acetylome

Daniel Mauvoisin, Florian Atger, Loïc Dayon, Antonio Núñez Galindo, Jingkui Wang, Eva Martin, Laetitia Da Silva, Ivan Montoliu, Sebastiano Collino, Francois-Pierre Martin, Joanna Ratajczak, Carles Cantó, Martin Kussmann, Felix Naef, and Frédéric Gachon

Supplemental Information

Supplemental Figures

Figure S1. Experimental design and data quality check, related to Figure 1

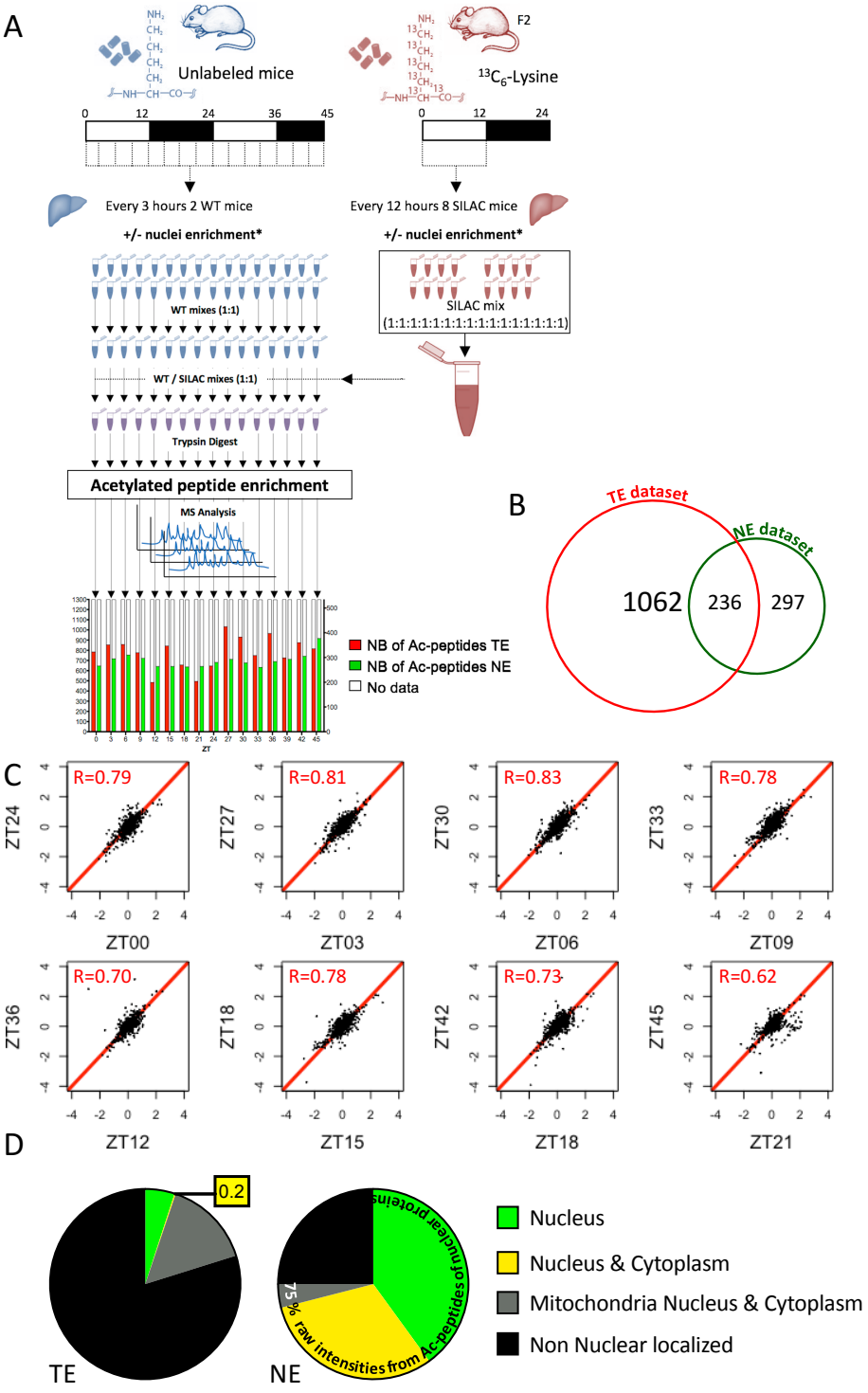

A. Workflow of the SILAC-based MS analysis of acetylated proteins from total mouse liver extracts (TE) and purified nuclei (NE). The lower graph represents the number of acetylation sites for each time point in TE (black bars, left Y axis) and NE (red bars, right Y axis).
B. Number of acetylated sites quantified in TE (red circle, 1298 acetylated sites identified) and NE (green circle, 533 acetylated sites identified).
C. Pearson correlation analysis of biological replicates at the eight time points. All values are log2 ratios to the common reference samples. The biological replicates are well correlated (76% average Pearson correlation) and showed similar spread, indicating that the quality of the protein purifications was fairly homogenous.
D. Fractions of raw intensity signals quantified with SILAC-MS for nuclear and non-nuclear located proteins in TE (left graph) and NE (right graph).

Figure S2. Overlap of rhythmic acetylation sites and expression of Acetyl-CoA synthesizing enzymes, related to Figure 2

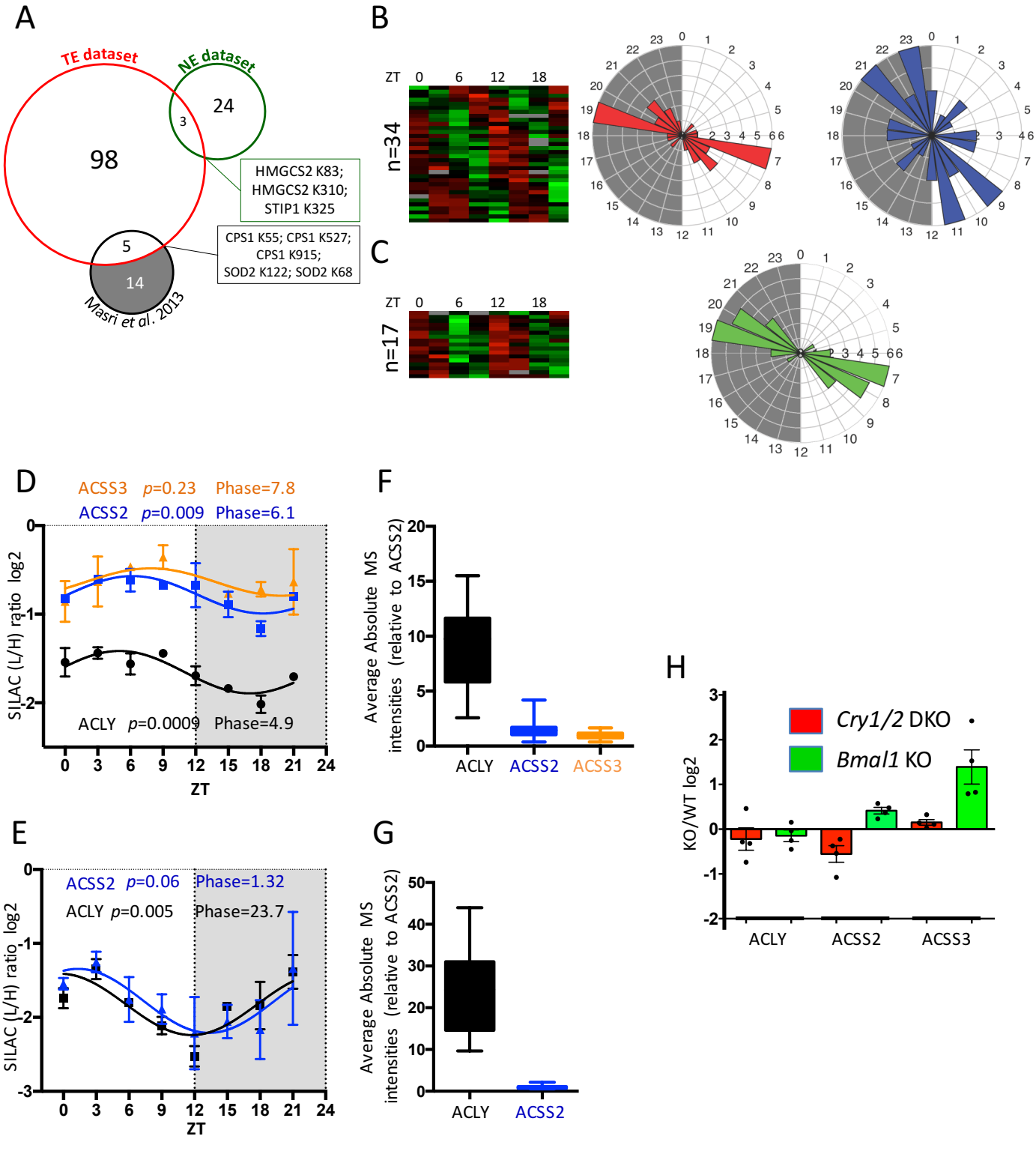

A. Venn diagram showing the overlap of rhythmic acetylation sites between the TE dataset (106 rhythmic acetylation sites), the NE dataset (27 rhythmic acetylation sites), and the dataset of (Masri et al., 2013) (19 rhythmic acetylation sites).
B-C. Heat maps showing 12 hours rhythmic acetylation sites normalized by their corresponding total protein amount in (B) TE (n=34) and (C) NE (n=17) under light-dark and night-restricted feeding conditions. Data were standardized by rows and gray blocks indicate missing protein data. The polar plots on the right of each heatmap display peak phase distribution of the 12 hours rhythmic acetylation sites in each extract. Colors indicate acetylation sites with a corresponding total protein having a defined mitochondrial (n=17 sites; red) or cytoplasmic (n=20 sites; blue) localization in TE, or acetylation sites from NE (n=17; green).
D-E. Temporal protein expression of ACLY (black), ACSS2 (blue), and ACSS3 (orange) in TE (D) and NE (E) (ACSS3 not detected in NE). The values represent the mean ± SEM from two independent biological samples.
F-G. Raw intensity signals quantified by SILAC-MS for ACLY (black), ACSS2 (blue), and ACSS3 (orange) in TE (F) and NE (G) (ACSS3 not detected in NE). Data are expressed relative to ACSS2 average signal, error bars represent min to max.
H. Differential protein expression level of ACLY, ACSS2, and ACSS3 in TE in *Cry1/2* DKO mice (red bars) and *Bmal1* KO mice (green bars) compared to respective WT animals. Data show average level ± SEM in four samples collected around the clock.
Data of panels D, F, H, and E, G are from (Mauvoisin et al., 2014) and (Wang et al., 2017), respectively.

Figure S3. Temporal nuclear expression of SIRT1 and SIRT7, related to Figure 3

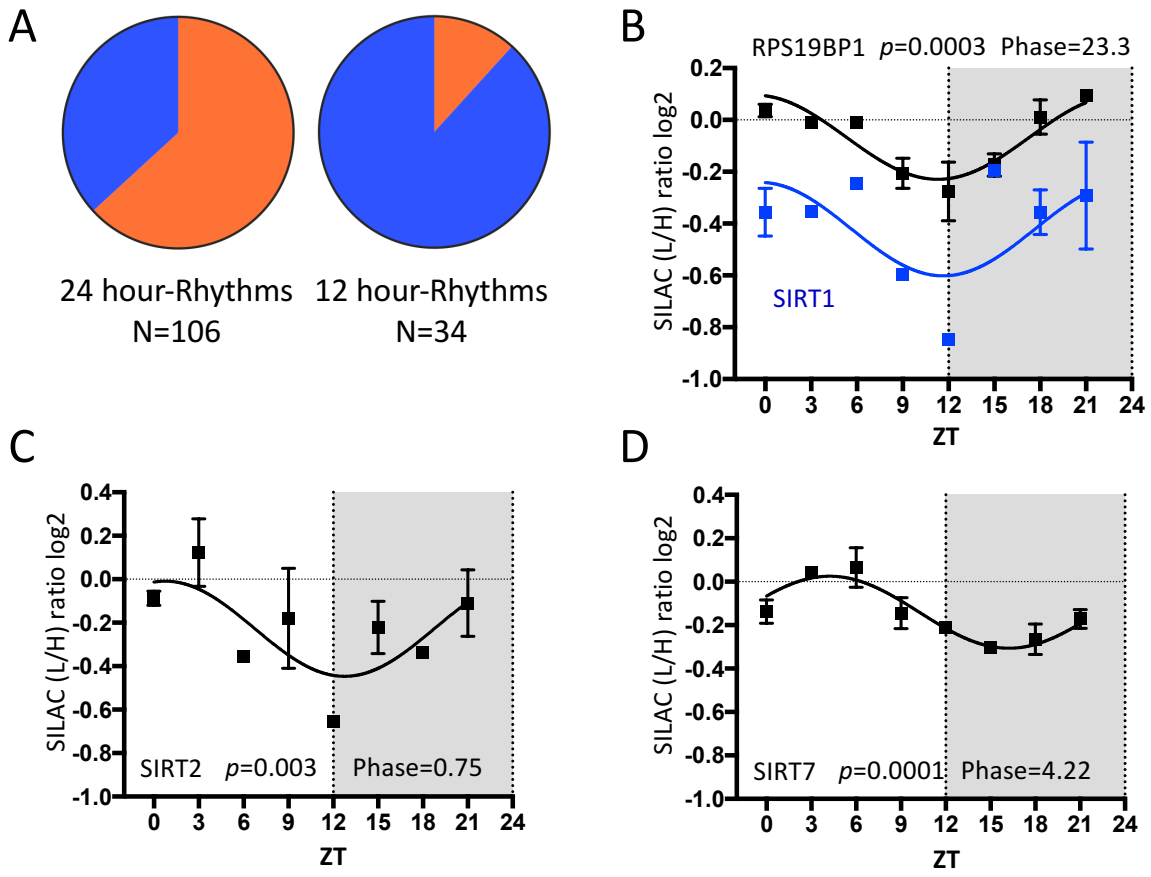

A. Proportion of SIRT3 targets (orange) versus non-SIRT3 targets (blue) in rhythmic acetylation sites with 24 hour-rhythms and 12 hour-rhythms.
B. Temporal nuclear expression of SIRT1 (blue) and its coactivator RPS19BP1 (black).
C. Temporal nuclear expression of SIRT2.
D. Temporal nuclear expression of SIRT7.
For B, C, and D, the values represent the mean ± SEM from two independent biological samples. Data are extracted from (Wang et al., 2017).

Figure S4. Additional metabolic pathways affected by rhythmic acetylation, related to Figure 5

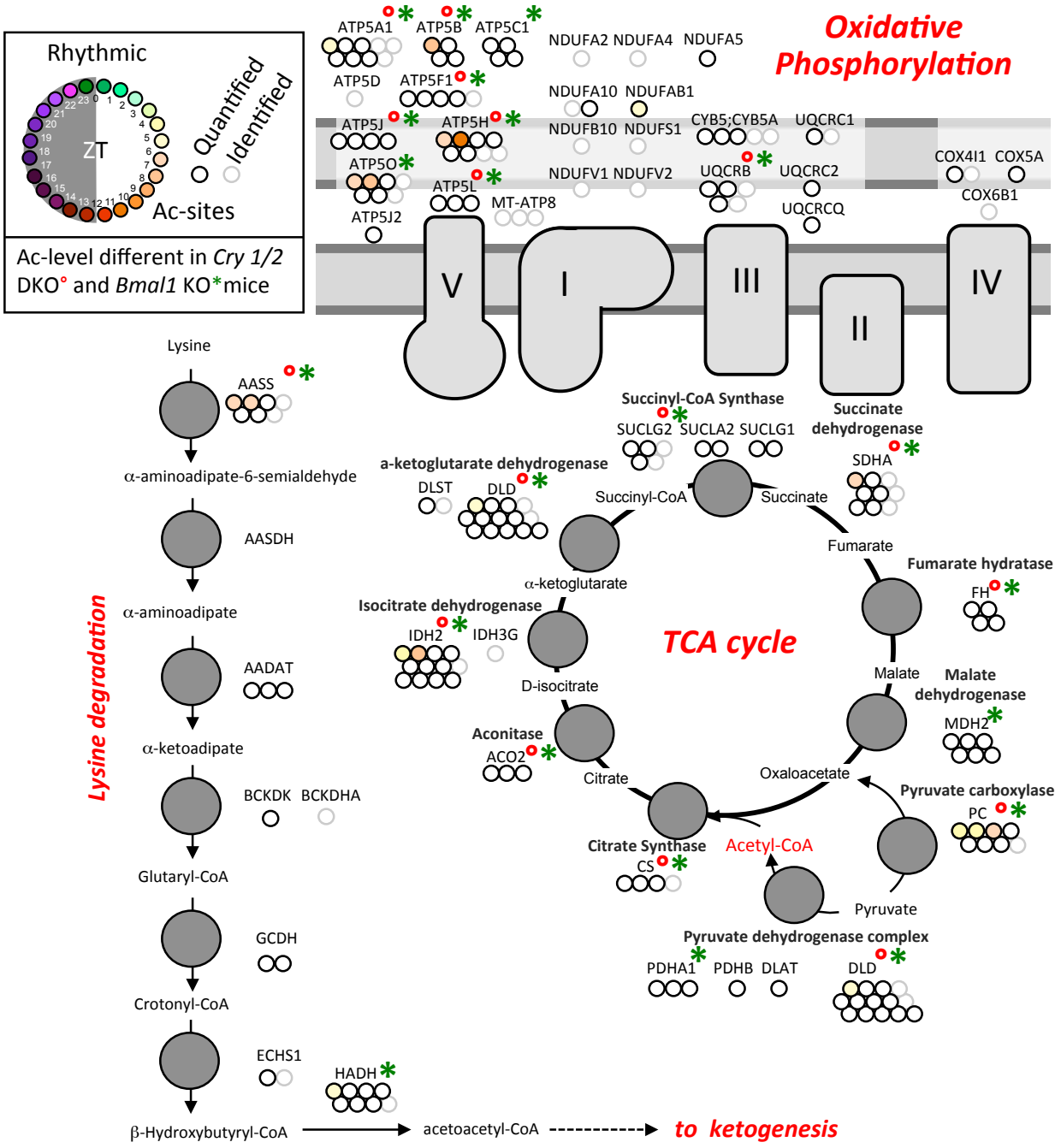

Rhythmic protein acetylation and their regulation by the circadian clock for lysine degradation, oxidative phosphorylation, and TCA cycle pathways. Each dot represents a unique acetylation site within the protein of interest. Grey and black dots represent non-rhythmic identified and quantified acetylation sites, respectively, whereas phase of rhythmic acetylation sites are color-coded. Superscripted red dots and green asterisks indicate protein acetylation level significantly different in *Cry1/2* DKO and *Bmal1* KO mice, respectively.

Figure S5. Differential acetylation of the enzymes involved in the different metabolic pathways in *Cry1/2* and *Bmal1* KO mice, related to Figure 5 and S4

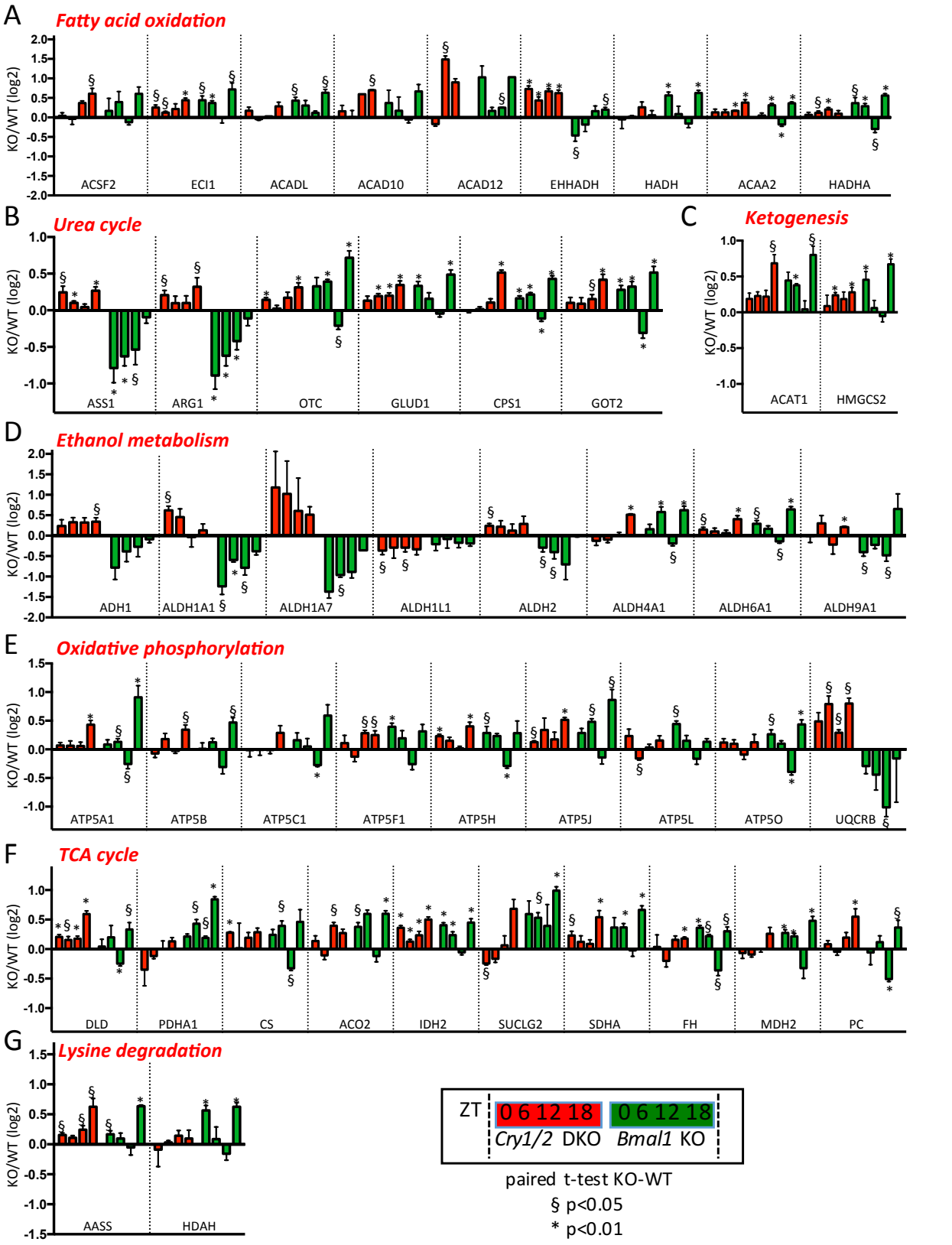

Differential temporal acetylation level of proteins implicated in the metabolic pathways presented in Figures 5 and S4: (A) Fatty acid oxidation; (B) Urea cycle; (C) Ketogenesis; (D) Ethanol metabolism; (E) Oxidative phosphorylation; (F) TCA cycle; and (G) Lysine degradation. Data shown for each protein represents mean differential level of global protein acetylation between *Cry1/2* DKO (red bars), *Bmal1* KO (green bars) and their corresponding WT controls (mean ± SEM of acetylation sites log2 difference). Paired student t-test was performed to compare global acetylation level of each protein between KO mice and their respective WT controls.

Figure S6. Impact of rhythmic acetylation on metabolites levels on additional pathways, related to Figure 6

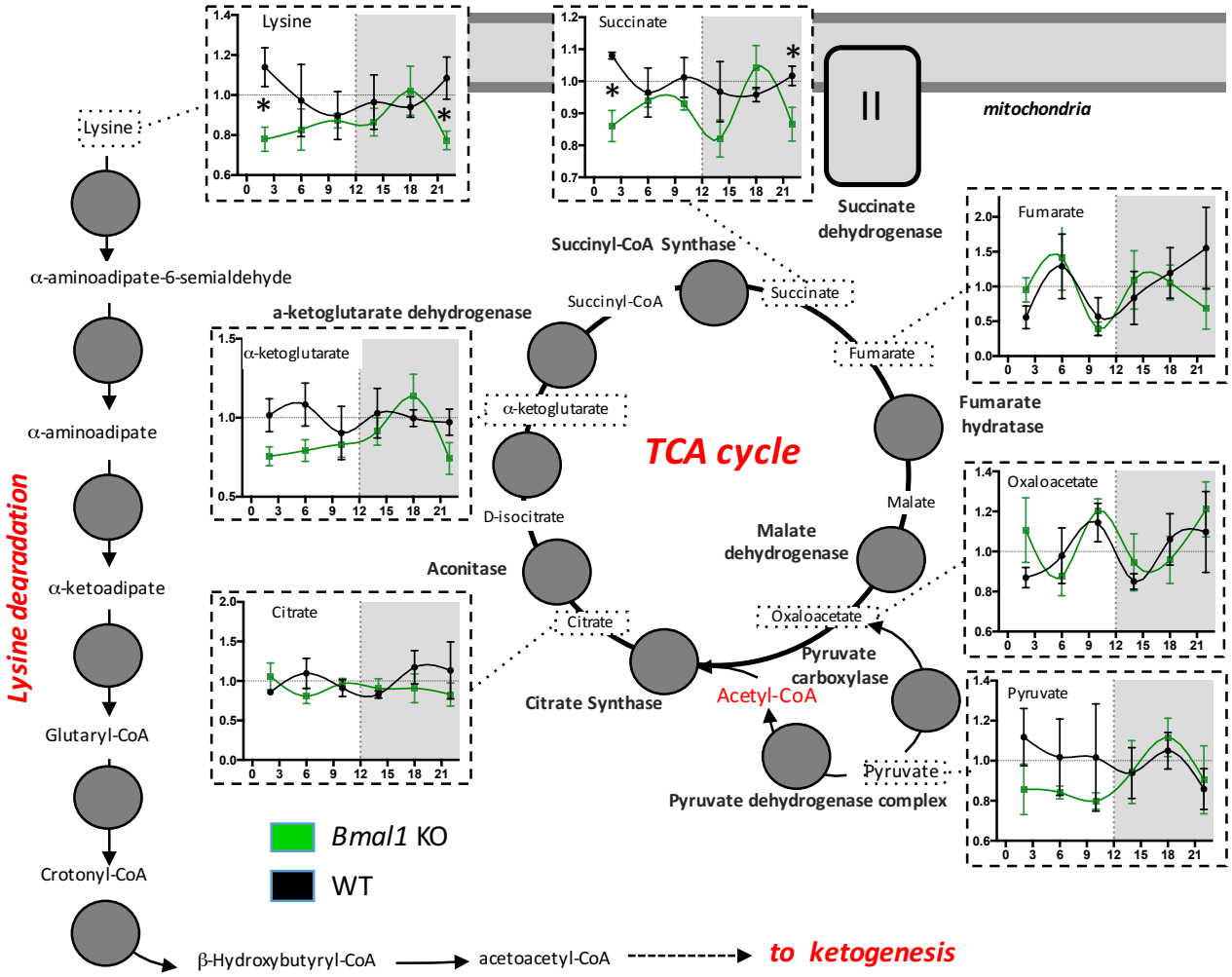

Liver temporal profiles of metabolites in *Bmal1* KO (green line) and WT littermates (black line). Data are expressed relative to the temporal mean of WT values ± SEM. The analysis concerned key metabolites of Lysine degradation and TCA cycle. Student t-test was performed to compare the average level of metabolites at every time point between the different genotypes (n=4). * indicate $p<0.05$ between *Bmal1* KO and WT mice.

Supplemental Experimental Procedures

Total protein extraction

Livers were homogenized in a lysis buffer containing 8M Urea, a protease inhibitor cocktail (cOmplete ULTRA®, Roche), a phosphatase inhibitor cocktail (PhosphoSTOP®, Roche), and HDAC and SIRTUIN inhibitors (AGK7, salermide, and trichostatin A, all from SantaCruz Biochemicals). After 20 min incubation on ice, extracts were centrifuged 10 min at 20,000 g. The supernatants were harvested and the resulting total protein extracts (TE) were quantified using a BCA protein assay kit (Thermo Scientific).

Nuclear protein extraction

Livers were homogenized in sucrose homogenization buffer containing 2.2 M sucrose, 15 mM KCl, 2 mM EDTA, 10 mM HEPES (pH 7.6), 0.15 mM spermin, 0.5 mM spermidin, 1 mM DTT, and protease inhibitors (0.5 mM PMSF, 10 mg/ml Aprotinin, 0.7 mg/ml Pepstatin A, and 0.7 mg/ml Leupeptin). Lysates were deposited on a sucrose cushion containing 2.05 M sucrose, 10 % glycerol, 15 mM KCl, 2 mM EDTA, 10 mM HEPES (pH 7.6), 0.15 mM spermin, 0.5 mM spermidin, 1 mM DTT, and protease inhibitors. After 45 min of centrifugation at 105,000 g at 4 °C, the nuclei pellets were suspended in a buffer composed of 10 mM HEPES (pH 7.6), 100 mM KCl, 0.1 mM EDTA, 10 % Glycerol, 0.15 mM spermine, 0.5 mM spermidine, 0.1 mM NaF, 0.1 mM sodium orthovanadate, 0.1 mM ZnSO4, 1 mM DTT, and protease inhibitors. This constitutes the purified nuclei fractions. Nuclear protein extracts were obtained by adding an equal volume of NUN buffer (2 M urea, 600 mM NaCl, 50 mM HEPES (pH 7.6), 1 mM DTT, a protease inhibitor cocktail (cOmplete ULTRA®), a phosphatase inhibitor cocktail (PhosphoSTOP®), and HDAC and SIRTUIN inhibitors (AGK7, salermide, and trichostatin A) followed by a 20 min incubation on ice. The supernatants resulting from a 10 min centrifugation at 21,000g at 4 °C constitute the nuclear extracts (NE). Protein extracts were quantified using a BCA protein assay kit (Thermo Scientific).

Analysis of acetylation by RP-LC MS/MS

Sample preparation for proteomic analysis

Equal amounts of proteins from TE or NE from 2 non-SILAC mice were pooled for each of the 16 time points (every 3 hours for 45 hours; WT mix). A complex and common reference SILAC protein mix (SILAC mix) was prepared from 16 SILAC protein samples (6 SILAC male and 10 SILAC female livers) collected at ZT0 and ZT12 (Fig S1A). Thereafter, the 16 mixes were obtained by adding the same amount of SILAC mix (250 µg for TE, and 175 µg for NE) to the WT mixes (125+125=250 µg for TE, and 87.5+87.5=175 µg for NE). An equivalent procedure was applied for the 4 *Cry1/2* DKO, the 4 *Bmal1* KO mice, and their 4 WT littermates protein samples collected every 6 hours for 24 hours (the same SILAC mix was used as a reference). Mixed heavy/light extracts representing each experimental condition (Fig S1A) were processed in parallel. Protein disulfide bridges were reduced with 10 mM tris (2-carboxyethyl) phosphine hydrochloride for 1 hour at 55 °C. Alkylation was performed with 17 mM Iodoacetamide for 30 min at room temperature in the dark. To remove lipids and salts, proteins were precipitated using methanol/chloroform. Briefly, methanol, then chloroform and water for adjusting final volume were added. Mixtures were centrifuged at 13,000 rpm for 5 min at 4 °C. Upper phases were discarded. The white precipitates were additionally washed with methanol prior to be dried for 5 min. Remaining pellets were suspended in 100 mM triethylammonium hydrogen carbonate buffer pH 8.5 and proteins were digested, first with Lys-C (1:100 *w*/*w*) (Promega) at 37 °C for 5 hours and then overnight with Trypsin (1:100 *w*/*w*) (Promega). Samples were cleaned up using Oasis HLB cartridges (Waters) and finally dried. Purified peptides were dissolved in the immunoprecipitation buffer (PTM Biolabs) for acetylated-lysine enrichment. A volume of 15 µL of drained anti-acetyl lysine antibody beaded agarose (PTM Biolabs) was washed with cold phosphate buffer saline. Peptides and washed beads were mixed and incubated overnight with gentle end-to-end rotation at 4 °C. The beads were centrifuged and the supernatant was discarded. After sequential washing of the beads with wash buffer I (PTM Biolabs) (3 times), wash buffer II (PTM Biolabs), and water (twice), the anti-acetyl lysine enriched peptides were eluted from the beads with elution buffer (PTM Biolabs), further dried and spin filtered (0.22 µm).

RP-LC MS/MS

The samples were dissolved in 25 µL H_2O/CH_3CN/Formic Acid 96.9/3/0.1 for RP-LC MS/MS analysis. RP-LC MS/MS was performed on a hybrid linear ion trap-Orbitrap (LTQ-OT) Elite equipped with an Ultimate 3000 RSLC nano system (Thermo Fisher Scientific). Proteolytic peptides (injection of 5 µL of sample) were trapped on an Acclaim PepMap 75 µm × 2 cm (C18, 3 µm, 100 Å) pre-column and separated on an Acclaim PepMap RSLC 75 µm × 50 cm (C18, 2 µm, 100 Å) column (Thermo Fisher Scientific) coupled to a stainless steel nanobore emitter (40 mm, OD 1/32") mounted on a Nanospray Flex Ion Source (Thermo Fisher Scientific). The analytical separation was run for 150 min using a gradient that reached 30% of CH_3CN after 140 min and 80% of CH_3CN after 150 min at a flow rate of 220 nl/min. For MS survey scans, the OT resolution was 120,000 (ion population of 1.10^6) with an *m/z* window from

300 to 1,500. For MS/MS with collision-induced dissociation at 30 % of the normalized collision energy, ion population was set to 1.10^4 (isolation width of 2 *m/z*), and a maximum injection time of 150 ms in the LTQ. A maximum of 20 precursor ions (most intense) were selected for MS/MS. Dynamic exclusion was set for 60 within a ± 5 ppm window. A lock mass of *m/z* = 445.1200 was used. Each sample was analyzed in triplicate.

Data processing and analysis

MaxQuant (version 1.4.1.2) (Cox and Mann, 2008) was used for data processing. Identification was performed using Andromeda (Cox et al., 2011) as search engine against the mouse UniProtKB database (26/06/2013 release; 50818 entries). Variable amino acid modifications were acetyl (K), acetyl (N-term), and oxidation (M). Carbamidometyl (C) was set as fixed modification. Trypsin/P (*i.e.*, cleaves after lysine and arginine also if a proline follows) was selected as the proteolytic enzyme, with a maximum of two potential missed cleavages (four missed cleavages parameter was also assessed but without any improvement on the results). Peptide and fragment ion tolerance were set to, respectively, 6 ppm and 0.5 Da. Peptide-spectrum match, protein and site false discovery rates (FDRs) were fixed at 1% against a reversed sequence database. Quantification was performed with stable isotope with a multiplicity of 2 using Lysine $^{13}C_6$ as heavy labels. A maximum of 3 labeled amino acids per peptide was specified. Site quantification used least modified peptide.

The mass spectrometry proteomic data have been deposited to the ProteomeXchange Consortium *via* the PRIDE (Vizcaíno et al., 2016) partner repository with the dataset identifiers PXD005317 and PXD005310 for TE and NE respectively.

^{1}H NMR spectroscopic analysis of liver Metabonome

Frozen liver samples (~40-60 mg) were homogenized in 650 µl of ice-cold methanol. Homogenates were incubated on ice for 15 min and then supplemented with ice-cold chloroform (650 µl), vortexed thoroughly, and incubated on ice for 15 min. Hence, 650 µl of water was added to each samples, vortexed thoroughly, and incubated overnight at -20 °C. Phase separation was performed by centrifugation at 13,000 g and 4 °C for 40 min. The upper soluble phases were collected and evaporated. The dried mouse liver extracts were homogenized in 700 µl of phosphate buffer solution (0.2 M $NaHPO_4$ pH 7.0, 90 % D_2O, 10 % H_2O) containing TSP (0.5 mM, reference signal at $\delta = 0$). After centrifugation, a volume of 600 µl was transferred into 5 mm diameter NMR tubes by using a Gilson robot (Gilson AG). ^{1}H NMR spectra were then recorded on a 600 MHz Avance II Bruker NMR spectrometer equipped with a 5 mm PATXI probe (Bruker Biospin) operating at 600.13 MHz and 300 K. Standard ^{1}H NMR one-dimensional pulse sequence with water suppression and Carr-Purcell-Meiboom-Gill (CPMG) spin-echo sequence with water suppression were acquired using 128 scans with 98 K data-points. Processing of ^{1}H NMR spectra was carried out using TOPSPIN 3.2 software package (Bruker Biospin). The spectral data (from $\delta = 0.4$ to $\delta = 10$) were imported into Matlab (version R2013b) and normalized to total area after solvent peak removal. Poor quality or highly diluted spectra were discarded from the subsequent analysis. Based on metabolic pathways of interest, representative signals of metabolites assignable on ^{1}H NMR spectra were integrated. The signals were expressed in arbitrary unit corresponding to a peak area normalized to total tissue metabolic profile, which is representative of relative change in metabolite concentration in the tissue.

References for antibodies used for Western Blotting

NRK1 antibodies were previously described (Ratajczak et al., 2016). Rabbit anti-SOD2/MnSOD (ab68155) and anti-SOD2/MnSOD (acetyl K68) (ab137037) antibodies were from Abcam. Rabbit anti-acetyl-lysine antibody (PTM-105), rabbit anti-succinyl-lysine antibody (PTM-401) and rabbit anti-malonyl-lysine antibody (PTM-901) were from PTM Biolabs.

Supplemental References

Cox, J., and Mann, M. (2008). MaxQuant enables high peptide identification rates, individualized p.p.b.-range mass accuracies and proteome-wide protein quantification. Nat Biotechnol 26, 1367-1372.

Cox, J.r., Neuhauser, N., Michalski, A., Scheltema, R.A., Olsen, J.V., and Mann, M. (2011). Andromeda: A Peptide Search Engine Integrated into the MaxQuant Environment. J Proteome Res 10, 1794-1805.

Masri, S., Patel, V.R., Eckel-Mahan, K.L., Peleg, S., Forne, I., Ladurner, A.G., Baldi, P., Imhof, A., and Sassone-Corsi, P. (2013). Circadian acetylome reveals regulation of mitochondrial metabolic pathways. Proc Natl Acad Sci U S A 110, 3339-3344.

Mauvoisin, D., Wang, J., Jouffe, C., Martin, E., Atger, F., Waridel, P., Quadroni, M., Gachon, F., and Naef, F. (2014). Circadian clock-dependent and -independent rhythmic proteomes implement distinct diurnal functions in mouse liver. Proc Natl Acad Sci U S A 111, 167-172.

Ratajczak, J., Joffraud, M., Trammell, S.A.J., Ras, R., Canela, N., Boutant, M., Kulkarni, S.S., Rodrigues, M., Redpath, P., Migaud, M.E., Auwerx, J., Yanes, O., Brenner, C., and Cantó, C. (2016). NRK1 controls nicotinamide mononucleotide and nicotinamide riboside metabolism in mammalian cells. Nature Commun 7, 13103.

Vizcaíno, J.A., Csordas, A., del-Toro, N., Dianes, J.A., Griss, J., Lavidas, I., Mayer, G., Perez-Riverol, Y., Reisinger, F., Ternent, T., Xu, Q.-W., Wang, R., and Hermjakob, H. (2016). 2016 update of the PRIDE database and its related tools. Nucleic Acids Res 44, D447-D456.

Wang, J., Mauvoisin, D., Martin, E., Atger, F., Galindo, A.N., Dayon, L., Sizzano, F., Palini, A., Kussmann, M., Waridel, P., Quadroni, M., Dulić, V., Naef, F., and Gachon, F. (2017). Nuclear Proteomics Uncovers Diurnal Regulatory Landscapes in Mouse Liver. Cell Metab 25, 102-117.